"Investigation on Degradation of Polymer solar cell"

A Thesis Submitted

In partial fulfillment of the requirement

For the degree of

MASTER OF TECHNOLOGY

IN

MATERIALS AND METALLURGICAL ENGINEERING

BY

ABHISHEK SHARMA

(Roll no. 600902001)

SCHOOL OF PHYSICS AND MATERIAL SCIENCE

THAPAR UNIVERSITY

PATIALA-147004, INDIA

CERTIFICATE

This is to certify that the thesis entitled **"Investigation on Degradation in Polymer Solar Cell"** submitted by **Mr. Abhishek Sharma** is in the partial fulfillment for Degree of MASTER of TECHNOLOGY in MATERIALS and METALLURGICAL ENGINEERING of this university. This work has been done under our supervision. The work presented in this thesis is original to the best of our knowledge and has not been submitted to any other degree of this or any other university.

This work has been carried out from 5 January 2011 to 12 July 2011.

Dr. Suresh Chand
Scientist G and Head
Organic and Hybrid Solar Cell Section
National Physical Laboratory
New Delhi-110012

Dr.D.P.Singh
Assistant Professor
School of Physics and Material Science
Thapar University
Patiala-147004

Dr.O.P. Pandey
Professor and Head
School of Physics and Material Science
Thapar University
Patiala-147004

Prof. S.K. Mohapatra
Dean. Academic Affairs
Thapar University
Patiala-147004

ACKNOWLEDGEMENT

*This master thesis work is the final examination toward getting my master degree in **Materials and Metallurgical Engineering** at **Thapar university (Patiala) Punjab**. The work has been carried out within **Organic and Hybrid Solar Cell Section** at **National Physical Laboratory (New Delhi) India**.*

*I express my deep sense of gratitude to **Dr. SURESH CHAND** for providing me an opportunity to work in Organic and Hybrid Solar Cell Section, NPL. His astonishing language skills and his clear vision of scientific content help me in tremendous manner. Words can hardly express my sense of gratitude to **Dr. PANKAJ KUMAR** for her invaluable supervision during the course of my thesis work. **Dr. PANKAJ** was always available and helpful. His great knowledge and wonderful attitude help in my training tremendously; his kindness, patience are much appreciable.*

*I want to express my deep sense of gratitude to my supervisor **Dr. D.P. Singh**. His wide knowledge and logical way of thinking have been of great value for me.*

*I express my gratitude to **Prof. O. P. Pandey,** Head, School of Physics and Material Science, Thapar University Patiala for his invaluable support and encouragement.*

*I am deeply indebted to my teachers**, Dr. Kulvir Singh**, **Dr.Puneet Sharma**, **Dr.Dinesh Bansal**, **Dr.Bhupendra Kumar Chudasama**.Their ideals and concepts have had a remarkable influence on my understanding in the field of Material Science.*

I would like to give my special thanks to all members of Organic and Hybrid Solar Cell Section at NPL for their kind support in my work.

I, also want to thanks my classmates at Thapar University,Patiala for their everlasting support .

I take pride of myself being son of ideal parents for their everlasting desire, sacrifice, affectionate blessings, and help, without which it would not have been possible for me to complete my studies.

Last but not least, I would like to express my gratitude to my God, without the help of who's this work was not performed.

Abhishek Sharma
Registration Number: 600902001

Abstract

Over the last few decades, Bulk Heterojunction Organic photovoltaic devices comprising an intimately mixed donor-acceptor blend have gained serious attention due to their potential forbeing cheap, light weight, flexible and environmentally friendly. In this thesis, P3HT/PCBM bulk heterojunction based organic photovoltaic devices with a normal geometry were investigated systematically. In initial studies we focused on optimization of the electrodes. We made devices with and without ITO. Apart from ITO, a thin layer of the conductive polymer PEDOT:PSS was chosen to be the transparent anode. Different PEDOT:PSS films with different thicknesses were characterized for their conductivity and transmission, work function also calculated with different PEDOT:PSS films. We did the degradation study of these devices and see the effect of PEDOT:PSS films thickness on the performance of ITO free solar cell solar cell.

The efficiency organic solar cell has been increased up to 8%, but the life time of these devices is only few hours in open atmosphere which is a measure drawback of organic solar cell. After making and characterizing these devices we saw that the life time of these devices was very low and this thing took our attention towards the degradation study of these devices. So we focused on degradation study of these devices and we found some interesting result after the complete degradation of these devices. The results have been discussed in detail.

Key words: Organic Semiconductor, Organic Solar Cell, Bulk Heterojunction

Table of Contents

Chapter 3: Fabrication of Organic Solar cells

Chapter 4 : Result And Discussion

Chapter 5: Conclusions Summary and Future plan

LIST OF FIGURES

Chapter 1

Chapter 2

Chapter 3

Chapter 4

Chapter1
Introduction

Energy source is the material basis of human activities, and it has been a key factor in the development of human society. Between the years 2020 and 2060, non renewable fossil fuels are expected to dwindle appreciably. Along with that combustion of fossil fuels contribute to many serious problems such as greenhouse effect, atmospheric pollution, and global warming which is thought to be caused by excessive carbon monoxide, chlorofluorocarbons (CFC's), and sulphur dioxide emissions. Therefore, search for some alternate inexpensive, environmentally sound, and renewable energy sources is an important step. Renewable energy is generated from natural resources such as sunlight, wind, rain, tides, and geothermal heat, which neither run out of support nor have any significant harmful effects on our environment **[1]**.

Among these renewable energy sources, the sunlight is remarkable in the sense that it could provide us the most considerable sum of energy: one hour's sunshine is already more than enough to satisfy worldwide energy needs for an entire year with the largest demand of human beings, which is near about 14 TW per year **[2]**. Over the 20^{th} century, human population quadrupled and energy consumption increase sixteen fold. It is estimated that there will be 8 to 10 billion people on Earth in 2050, with a 14 TW energy gap **[2]**. Obviously, solar sources will be the best way to offset the gap. As a kind of technology which can convert sunlight directly into electricity without emitting carbon dioxide and can thereby help to combat global warming, solar cells (also called photovoltaic) have gained broad interest both in the academic and industrial community **[3-7]**. Solar cells can be used in a larger range of locations. Even in regions where the sky is often cloudy, batteries can store the energy produced from the solar cells and the stored energy in batteries can be utilized during dark.

Solar energy is by far the renewable energy source with the greatest potential (Table 1). It has the ability to cover the world's energy demand several thousand times and unlike fossil fuels, solar energy is readily available world-wide.

Table 1. Energy available for harvesting from different sources compared to the global energy demand [8, 9].

Global consumption	Hydro	Geothermal	Wind	Solar
15 TW	7. 2 TW	32 TW	870 TW	86,000 TW

The energy from sunlight that strikes the Earth in one hour exceeds the annual human energy consumption on the planet. Therefore, extracting energy directly from sunlight has been acknowledged as an essential means to diversify future global energy production. Fig. 1.1 shows the relative size of earth compared to that of sun. The photograph is taken from website of NASA. The diameter of sun is about 109 time diameter of earth. The amount of solar energy from the sun to the earth is gigantic, i.e. $3x10^{24}$ J per year, about 10^{4} times more than what mankind consumes currently.

.

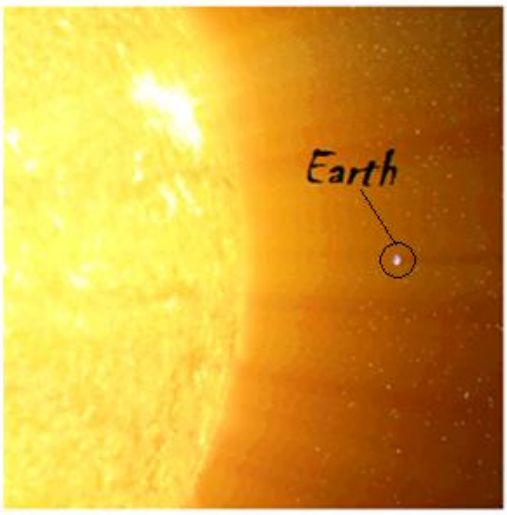

Figure 1.1: The relative size of earth compared to sun (from NASA).

Solar energy emitted by the sun and reaching the earth's surface is in the form of electromagnetic radiation that is available over a wide spectral range (300-2100 nm). In order to be used, the radiation needs to be converted into an energy form suitable for our needs.

Four different types of solar energy conversion methods are currently available for this purpose. **Thermal solar energy conversion** represents as one of the best solar energy harvesting which involves the conversion of solar radiation for direct heating of water in domestic usage. **Thermoelectric solar energy conversion** involves the use of solar energy to heat water to generate steam required to rotate electricity producing turbines in power plants. **Chemical solar energy conversion** represents the conversion of solar energy into chemical energy. Whereas **photoelectric solar energy conversion** represents the conversion of solar light directly into electricity. The devices used for photoelectric conversion are known as solar cells or photovoltaic devices.

1.0. Solar energy conversion and solar cells

Due to its abundance the solar energy is now becoming one of the primary sources of energy as an alternate to fossil fuels. The versatility, abundance and environmental friendly nature have made it one of the most promising renewable sources of energy. Solar cells convert the solar energy into electrical energy to drive various electronic appliances. Since the first crystalline silicon based solar cell was developed at Bell Laboratories **[10],** solar cell technologies have been studied extensively. So far, traditional in p-n junction solar cells can harvest more than 20 % **[11]** of the incoming energy, which is already close to the theoretical upper limit of 30 % **[12].** Silicon-based solar cells represent the most widely established solar cell technology which currently occupies more the 85% of the market **[13]**. Although, photovoltaic technology has been on the market for many years, less than 0.1% of the total world energy production is based on it.

A major obstacle is the relatively high production cost of silicon-based technology when compared to other sources of energy. The fabrication of inorganic devices requires intensive processing at high temperatures as well as high vacuum conditions and requires a large number of lithographic steps. Solar cells are therefore not widely used for commercial electricity production because they cannot compete with fossil fuels or other renewable energy sources as seen in (Figure 1.2). Therefore, in order to fully explore the potential of photovoltaic technology, new materials have to be developed.

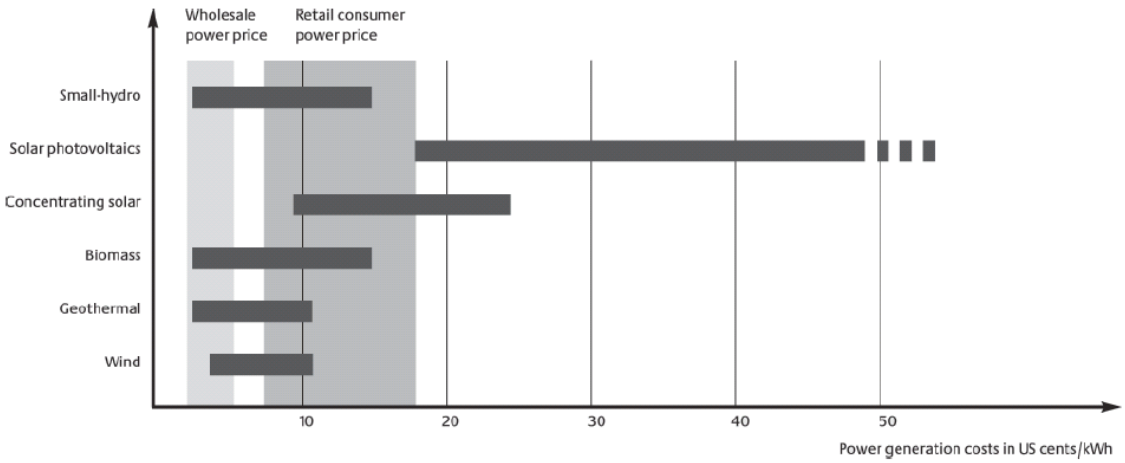

Figure 1.2 Prices of electricity produced from different renewable energy sources [14].

Introduction of polymers to solar cells is a promising candidate for low manufacturing cast of solar cells **[15]**. Their solubility means that they are easy to process. Polymer solar cells have been studied intensively in recent years. The present power conversion efficiency (PCE) of bulk heterojunction (BHJ) based polymer solar cells has exceeded 7 % **[16]**, but it is still much below the value for inorganic solar cells, and in addition, their lifetime is significantly shorter. However, organic photovoltaic technology shows great promise for decreasing the cost of solar energy. The semiconducting materials that comprise the active layer of organic solar cells are polymers or small molecules, which potentially are much cheaper to prepare and process than inorganic materials thanks to straight forward fabrication method such as roll-to-roll (R2R) print. Furthermore, this technology offers the possibility for thin, flexible, lightweight devices due to the superior mechanical characteristics of many organic materials; especially polymers.

1.0.1. Working mechanism of a solar cell

Photovoltaic cells generate useful electric energy from sun light through multiple steps of energy conversion processes. Light is made up of packets of energy, called photons, whose energy depends on the frequency, or colour of the light. The solar spectrum covers ultra violet to infrared wavelength ranges. Only 30% of incident light energy is in the visible light range, while over 50% is in the infrared range. The photons in UV and visible range have enough energy to pump electrons in semiconducting material, and this can be effectively

used for charge generation (see in Fig 1.3). However, IR waves are too weak to generate electricity using conventional PV technology. The photovoltaic effect was discovered in 1839 by Edmund Becquerel, a French experimental physicist who experimented with an electrolytic cell made up of two metal electrodes. Becquerel found that certain materials produced small amounts of electric current when exposed to light. In 1905, Einstein explained the photoelectric effect, which established the foundation for a theoretical understanding of the photovoltaic effect. When photons in the UV range are illuminated on a metal surface, free electrons escape from the metal surface due to excitation by incident light. They are then ejected into the atmosphere.

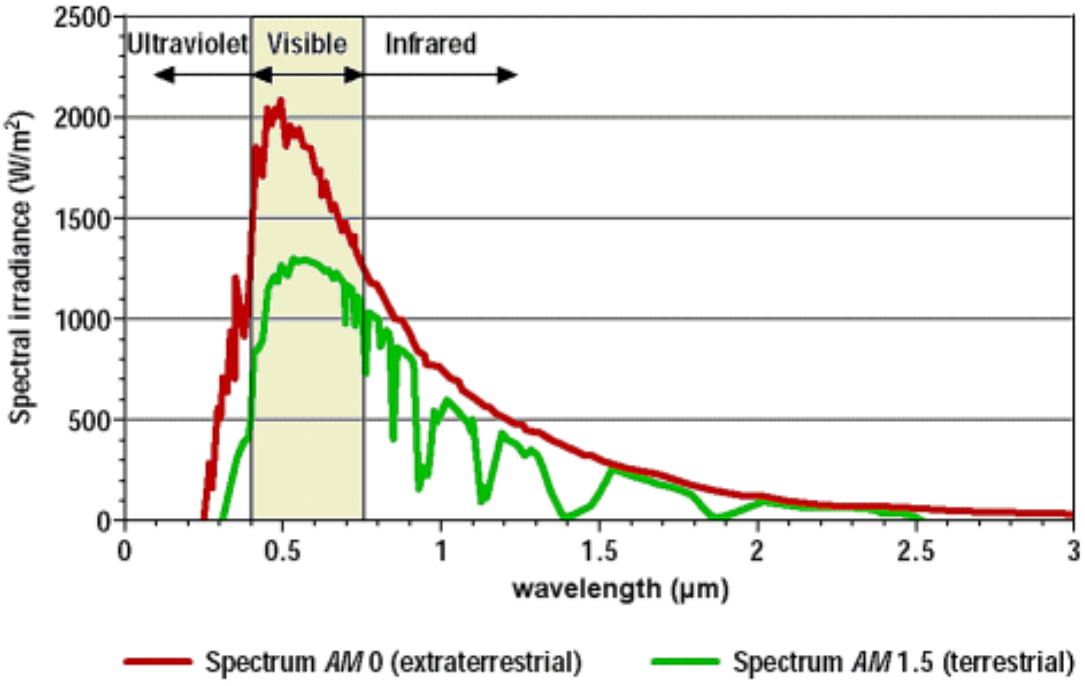

Figure 1.3: Solar spectrum

In most cases, when absorbed photons in a material pump ground state electrons to the excited state the excited electrons promptly relax to the ground state. However, in photovoltaic devices, the excited electrons and the produced hole in the ground state should be collected separately to produce power. The photovoltaic process is composed of four steps: light absorption, charge generation, charge transport, and charge collection **[17]**. Light absorption occurs when the material has a semiconducting property that responds to incident

waves. The absorption characteristic is dependent on the band gap of the semiconducting material and its intrinsic extinction coefficient. The next step is charge generation. When the incident photon hits electrons at the ground state in inorganic semiconductors generate, free carriers are generated. However, in organic semiconductors, excited electrons slightly relax and then form an excitons, a bounded electron and hole pair. To make an efficient organic photovoltaic cell, effective dissociation of excitons is a key issue because the binding energy of the excitons is large **[18]**. Once the excitons are dissociated the next step is the charge transport process, involving the transport of dissociated charges to electrodes through charge transporting pathways. During the charge transport, if the transporting medium has defects such as charge traps or barriers that hinder charge transport, cell performance decreases. Removing this loss mechanism during the transport process should be achieved to improve the cell performance.

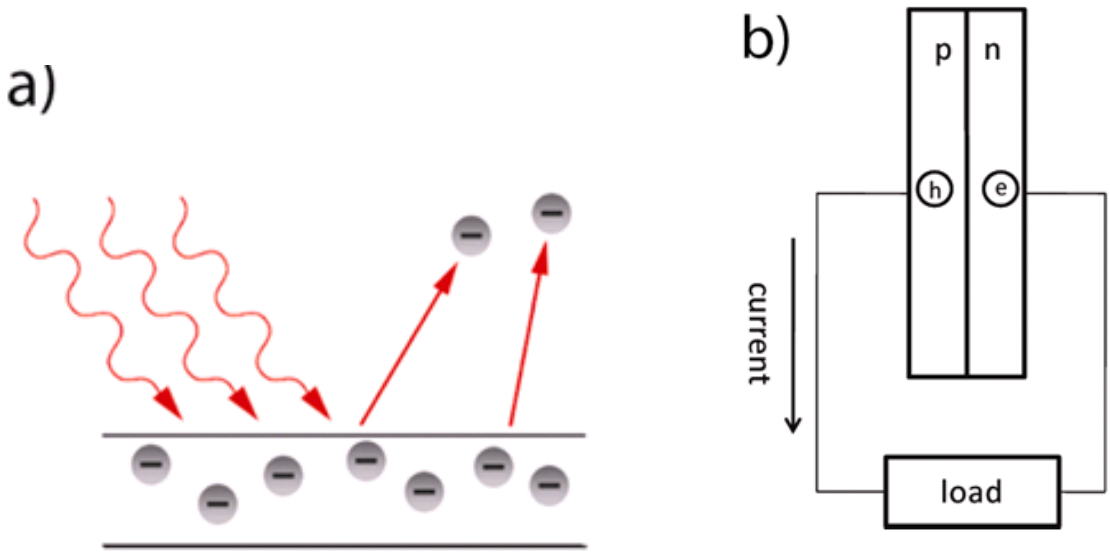

Figure 1.4: (a) Photoelectric effect and (b) Photovoltaic effect

The final step is the charge collection, which occurs when the transported charges are collected from the semiconductor to the cathode or anode at the interface. When the interface is not carefully optimized, it may cause a dissipating sink of the transported charges.

1.1. Organic semiconductors

Chemically, polymers are formed by repetitive covalent bonding of chemical units or monomers. Molecular weights over 10,000 g mol^{-1} are possible and therefore they are often referred to as "macromolecules". Polymers are thought to be insulators and generally not to considered as interesting electro-optic materials. This attitude has changed during last three decades starting with the discovery of high electrical conductivity in polyacetylene. Reporting the metallic properties in polyacetylene in 1977, Heeger, MacDiarmid and Shirakawa paved the way for a new kind of material: electronically conducting polymers. They discovered that chemical doping of conjugated polymers results in an increase of electronic conductivity by several orders of magnitude. This work was honoured by the Nobel Prize in chemistry in 2000 **[19]**. The conjugated polymers possess semiconducting character and therefore called organic semiconductors. During the last 25 years, a tremendous amount of experimental and theoretical work was been devoted to analyzing the electrical, physical, structural and optical properties of these materials. Consequently, they are today used in various applications, like biosensors, light - emitting diodes, solar cells, photodiodes, transistors, etc.

1.1.1 The semiconducting behaviour of conjugated polymer

Based on the type and number of carbon atoms along the main chain, polymers can be divided into two major classes: saturated and unsaturated. A saturated polymer has no double bonds, while unsaturated defines polymers which contain double bonds. Most conductive polymers have an unsaturated structure. Conjugated means that the back bone carbon chain is unsaturated and therefore has alternating double and single bonds. The valence electrons of carbon atoms in molecules having conjugated π-electron systems are sp^2-hybridized. Fig. 1.5 shows the spatial electron distribution leads to an overlap of the p_z as well as of the sp^2 orbitals of adjacent carbon atoms resulting in molecular π- and σ-bonds, respectively. During the transition from the atom to the molecule, the p_z atomic orbitals split into a bonding (π) and anti-bonding (π^*) orbitals which are energetically separated within a few eV. The energetically highest occupied bonding orbital in organic semiconductors is called highest occupied molecular orbital (HOMO) and the energetically lowest unoccupied anti-bonding orbital - usually indicated as the π^* orbital - is called LUMO.

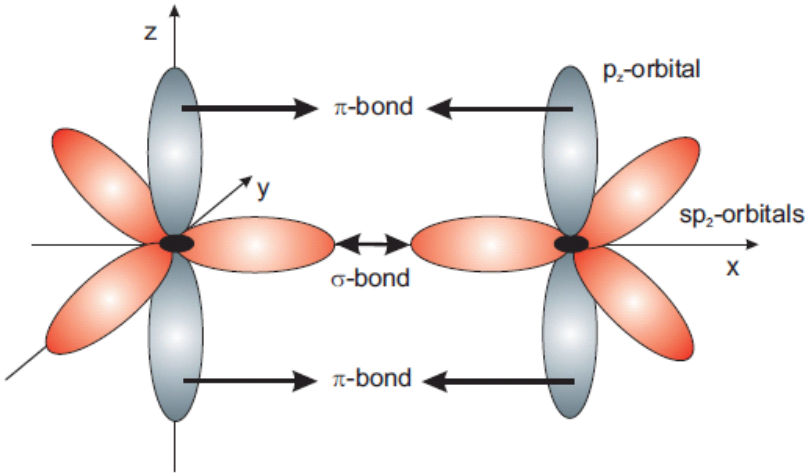

Figure 1.5: sp^2-hybridization of the valence electrons of two carbon atoms lead to molecular pi and sigma bondings.

The lower bonding π- orbital is equivalent to the valence band of an inorganic semiconductor, and the higher energetic π*- orbital forms the conduction band. Fig. 16 (a) shows the energy levels of a π-conjugated molecule, the lowest electronic excitation is between the bonding π-orbital and the antibonding π*-orbital. The difference between these two energy levels is called 'band gap' (see in Fig 1.6(b)). The optical and electrical properties of a material are related to this band gap. The electronic excitation with the lowest energy is therefore taking place as a electronic $\pi - \pi^*$ excitation. Due to the energy gap in conjugated polymers, these materials could absorb or fluoresce in the visible, near infrared or near UV spectral range and are therefore used in photovoltaic or light emitting applications.

Hypothetically the electron populating the p_z orbital's of the carbon atom in a linear sp^2 carbon chain are delocalized and create half filled valance band. This would predict a metallic ground state for these materials. In this linear chain, the overlapping sp^2 - hybridized orbitals of the carbon atoms form *s* bonds, and the remaining out of plane p_z orbitals, each occupied by one electron, overlap with neighbouring p_z orbitals to give π - bonds.

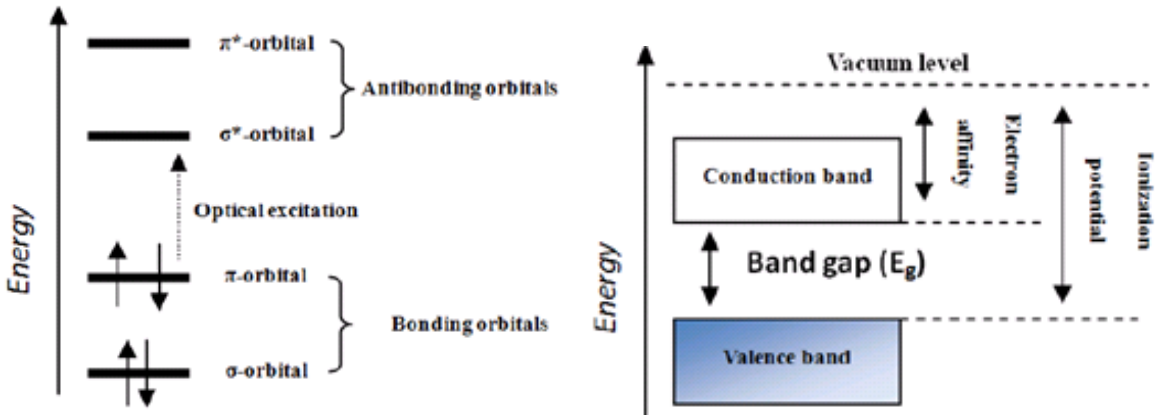

Figure 1.6: (a) The energy levels of a π-conjugated molecule, the lowest electronic excitation is between the bonding π-orbital and the antibonding π*-orbital, (b) collection of molecular orbitals form bands separated by an energy gap.

Though the chemical structures of these conjugated polymers propose alternating single and double bonds, the electrons that constitute the π – bonds are not localized but extend over several adjacent atoms due to the isomeric effect. Fig. 1.7 shows the molecular structure of polyacetylene, a most important conjugated polymer. Most organic polymers are hole conductors.

Figure 1.7: Isomeric structures of polyacetylene

This means that charge carriers are mostly empty states (holes) in the valance band. They are referred as ‘p - type’. On the other hand, materials with electrons as charge carriers in the conduction band are called ‘n - type’. In organic solar cells, the doping is induced by a photo-induced electron transfer from the lowest unoccupied molecular orbital (LUMO) of a donor to the lower lying LUMO of an electron – acceptor molecule. Usually, conjugated polymers have a band gap around 2 eV, which is rather high in comparison to commonly used inorganic semiconductors used for photovoltaic applications. This leads to a limited

absorption spectrum, which does not fit the maximum of the solar emission spectrum, located between 600 and 800 nm.

1.2. History of Organic Solar Cells

1.2.1 Single layer organic solar cell

The single layer device structure of organic photovoltaic (OPV) cells is comprised of a transparent electrode/organic photosensitive semiconductor/electrode (see Fig. 1.8). In 1994, this structure was created by R. N. Marks *et al*. using 50-320 nm thickness of poly (*p*-phenylene vinylene) (PPV) sandwiched between an ITO and a low work function cathode. The reported quantum efficiencies for this device were around 0.1% under 0.1mW/cm^2 intensity **[20].** This low quantum efficiency resulted from intrinsically low mobility of charges through semiconducting organics. The carrier mobility of semiconducting organics remains around 10^{-3} cm^2/V·s, while the mobility of single crystalline silicon is about 10^3 cm^2/V·s order. This indicates that the photo-generated charges in semiconducting organics require more time to be collected from electrodes. The slow charge transport itself decreases the efficiency of the OPV cell, but also increases the recombination chance of charges in the device. The other problem that causes the low PCE of OPV cells is exciton formation, which are strongly bound dipole charges **[21]**.

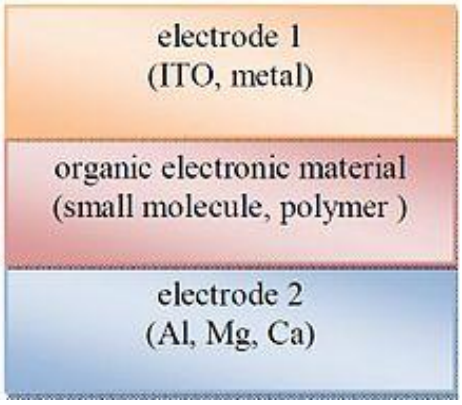

Figure 1.8: Structure of single layer organic solar cell

Free electrons and holes are desired as an efficient charge carrier because the bound exciton requires an additional exciton dissociation step to make free carriers, which can decrease the carrier generation efficiency. In a single layer OPV cell, only one place to dissociate excitons into free carriers is the interface between semiconducting organics and a cathode. Later, it was known that the excitons are more efficiently dissociated at the interface between donor and acceptor, and a bilayer OPV cell was developed by inserting an acceptor layer between a donor semiconducting organic and the cathode.

1.2.2 Bilayer Organic Solar Cell

The bilayer OPV cell structure includes an additional electron transporting layer than is found in the single layer OPV structure (see in Fig 1.9). This structure was first realized by C. W. Tang in 1986 and the device structure was comprised of indium tin oxide (ITO)/ copper phthalocyanine (CuPc)/ perylene tetracarboxylic derivative (PV)/ silver (Ag) **[22]**. The reported PCE was 1% under simulated AM2 conditions. This ten-fold PCE increase, resulted from improving exciton dissociation efficiency by adding electron transporting material that forms an offset energy band with hole transporting material. However, the reported PCE of bilayer OPV cells is still significantly lower than that of inorganic based PV cells. One reason for this is the intrinsically short excitons diffusion length of excitons in organic semiconductors, which are typically around 10-20 nm **[23,24,25]**.

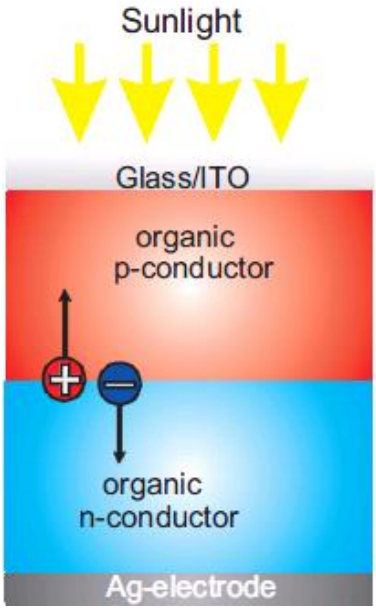

Figure 1.9: Bilayer structure of an organic photovoltaic device.

Researchers attempted to overcome this limitation in the bilayer OPV cell by using buckminsterfullerene, C_{60} in which the exciton diffusion length is around 20 nm. P. Peumans *et al.* replaced perylene tetracarboxylic derivative with C_{60} as an acceptor in the device structure and the device produced 3.5 % PCE **[26]**. This improvement of PCE is attributed to the longer travel distance of excitons in the triplet state of C_{60}.

However, since donor and acceptor layers are around 40-60 nm thickness, most of the absorbed photon energy is not efficiently converted into free carriers and dissipated by recombination, which indicates that photo generated excitons are dissociated only near the interface between donor and acceptor. Other approaches to building bilayer OPV cells using conjugated polymers. Sariciftci *et al.* fabricated the first bilayer OPV cell that used a conjugated polymer where the hole transporting material was MEH-PPV and the electron transporting material was C_{60}. In this structure, MEH-PPV plays a role in both absorbing photons and transporting holes to an anode, and C60 transports electrons to a cathode **[27]**.

1.2.3 Bulk Heterojunction OPV Cells

Since bilayer OPV cells collect very small amounts of excitons created near the interface of donor and acceptor, bulk heterojunction OPV cells, which have an intermixed composite of donor and acceptor, have an advantage in terms of having much larger interface area between donor and acceptor materials resulting more photon harvesting and enhanced efficiency (see in Fig(1.10)). For the first time, Yu *et al.* investigated a phase-separated polymer blend composite made of poly[2-methoxy-5-(2'-ethyl-hexyloxy)-l,4-phenylene vinylene] (MEH-PPV), as a donor and cyano-PPV (CN-PPV) as an acceptor **[28]**. The photo-luminescence and electroluminescence of both component polymers was quenched in the blend, which is indicative of rapid and efficient separation of photogenerated electron hole pairs with electrons on the acceptor and holes on the donor. Diodes made with such composite semiconducting polymers as the photosensitive medium show promising photovoltaic characteristics with energy conversion efficiency of 1.5 %, which is much larger than that of diodes made with pure MEH-PPV.

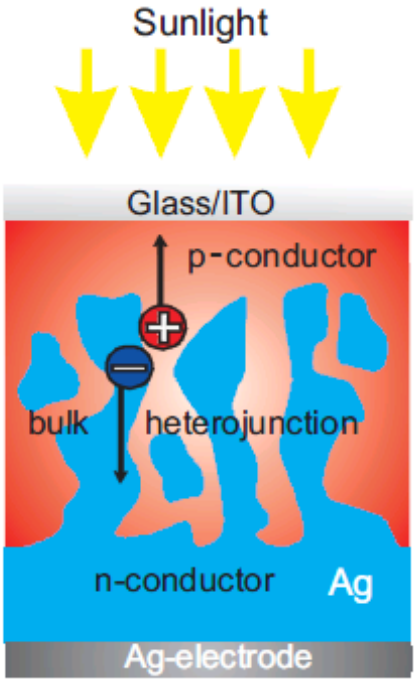

Figure 1.10: Bulk hetrojunction structure of organic photovoltaic device.

The next significant improvement in PCE of blend OPV cells was achieved using poly (3-hexylthiophene) (P3HT) as a hole transporting polymer. Gang Li *et al.* fabricated a blend OPV cell using P3HT and phenyl [6,6] C_{61} butyric acid methyl ester (PCBM) (a soluble derivative of C_{60}). The significant improvement in PCE, results mainly from the crystallinity of P3HT **[29]**. After casting P3HT and PCBM blend solutions on PEDOT:PSS/ITO, the blend film morphology was controlled by varying the evaporation rate. During the solvent annealing, P3HT and PCBM formed a well-mixed, interdigitated blend film where P3HT forms fibril-like crystalline morphology and PCBM aggregates are embedded. This phase separated morphology of blend layers enhances the hole mobility of the conjugated polymer, and also improves the absorption efficiency from the fibril-like P3HT aggregates. The best performance from the optimized blend OPV cell was 4.4 %. Kim *et al.* also investigated a similar blend OPV structure focused on the regioregularity of P3HT **[30]**. They prepared various P3HT and PCBM blend solutions in which P3HT had different regioregularities ranging from 80% to 96%. The fabricated devices were thermally annealed to induce phase separation of P3HT and PCBM. The investigation revealed that a higher order of regioregularity of P3HT helps to form the crystallized fibril-like shape of P3HT, which improves charge transport as well as light absorption efficiency.

1.3. Fundamental physical processes in Organic Solar cells

The working mechanism of an organic solar cell, involves five basic fundamental physical processes:

1. Creation of excitons,

2. Diffusion of excitons,

3. Dissociation of charge carriers at the donor/acceptor interface,

4. Charge transport, and

5. Extraction of the charge carriers at the electrodes,

These processes have been discussed in detail in the following sections.

1.3.1 Creation of Excitons

Since solar irradiation reaching the earth's surface varies greatly with a lot of factors, the photovoltaic industry, in conjunction with the American Society for Testing and Materials (ASTM) and government research and development laboratories, has developed and defined a standard terrestrial solar spectral irradiance distribution "AM1.5G" for theoretical evaluation of the solar irradiation effects and for simulator design.

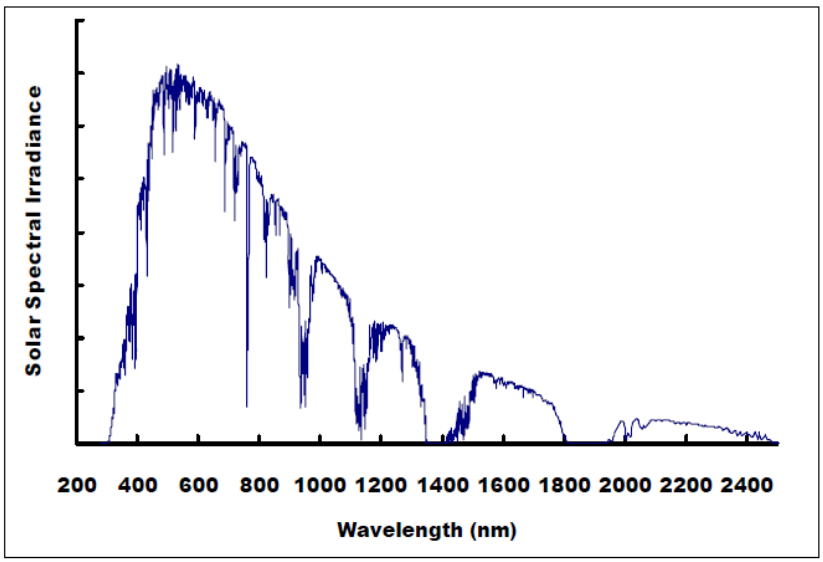

Figure 1.11: The standard AM 1.5G solar spectrum

In the AM 1.5 spectra (Figure 1.11), solar radiation covers a wide range of wavelengths, with the maximum irradiation at 480 nm and 70% of the photons located in the range of 400-920 nm.

Most solution processable semiconducting polymers have band gaps larger than 1.9 eV, indicating that only 30% of the solar photon flux is covered. Because most polymers have low charge-carrier mobility, the thickness of the active layer is limited to about 100 nm, which in turn leads to the absorption of only about 60 % of the incident light at the absorption maximum (without considering the loss from the back reflection of the electrode) **[31]**. So, the organic materials with expanded absorption spectra up to 700-800 nm and high charge-carrier mobility are favourable for efficient solar cells. Upon light absorption in organic materials, the exciton, a Coulomb-correlated electron-hole pair, is generated. When a photon enters a semiconductor, an electron is excited from the valence band into the conduction band (see Fig 1.12).

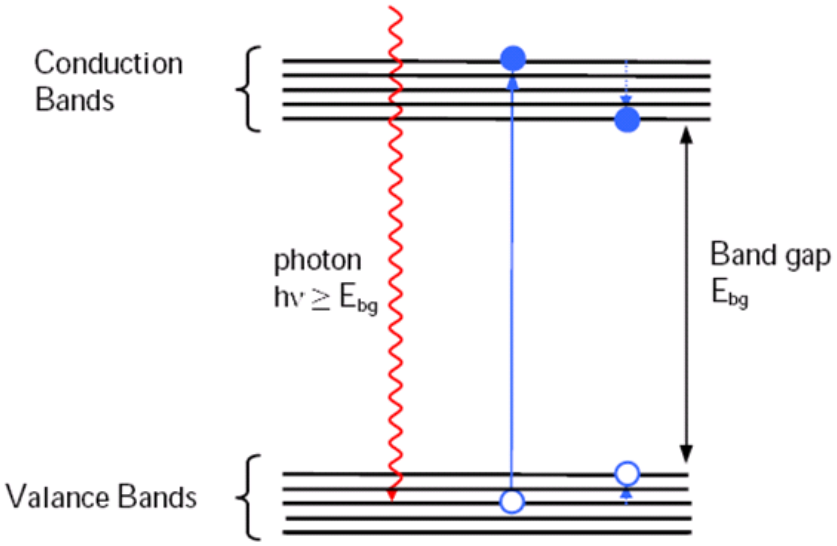

Figure 1.12: Charge separation due to the photon absorption

The missing electron in the valence band leaves a hole (of opposite electric charge) behind, to which the electron is attracted by the Coulomb force **[32]**.

1.3.2 Diffusion of Excitons

After the excitons are generated, they need to firstly dissociate to the donor/acceptor interface for the charge separation. Since the excitons dissociation process is confined to the D/A interfacial area, only excitons produced at a distance shorter than their diffusion length have the good possibility to reach the D/A interface where charge carriers are formed. Hence, for polymer-based solar cells, the excitons diffusion length L_D is an important parameter because the excitons diffusion process masters the photo-excitation energy transfer to the D/A interface. Consequently, the maximum thickness of the active layer is limited by the exciton diffusion length, and thus the maximum fraction of the incident light that the cell can absorb is also restricted. The exciton diffusion length L_D is defined as

$$L_D = \sqrt{D\tau_0}$$

where D is the diffusion constant and τ_0 is the decay time constant. So far two methods have been usually applied to estimate the exciton diffusion length L_D for organic materials. The exciton diffusion lengths in various conjugated polymers reported in the literature, differ very much, ranging from 5 to 20 nm **[33,34]**.

1.3.3 Dissociation of Charge Carriers at the Donor/Acceptor Interface

The key process after the exciton diffusion is the dissociation of excitons into free charge carriers. This process can be explained in the following two steps. One of the main differences between inorganic and organic semiconductors is the magnitude of the exciton binding energy, i.e. the strength of the Coulomb attraction between the electron and hole. In many inorganic semiconductors, the binding energy is smaller than the thermal energy (kT) at room temperature and therefore free charges are created under ambient conditions upon excitation **[35],** whereas the exciton binding energy in an organic semiconductor exceeds kT and consequently the excitons are formed upon excitation instead of free charges **[36]**. The method to dissociate bound electron-hole pairs in organic semiconductors then is the so-called donor/acceptor interface. Once an exciton reaches the D/A interface, the electron promoted into the LUMO level of the excited donor can be transferred to the lower-lying

LUMO level of the acceptor. The hole then remains on the HOMO level of the donor, therefore light is converted by this photo-induced electron-transfer process into electrical charges **[37]**.

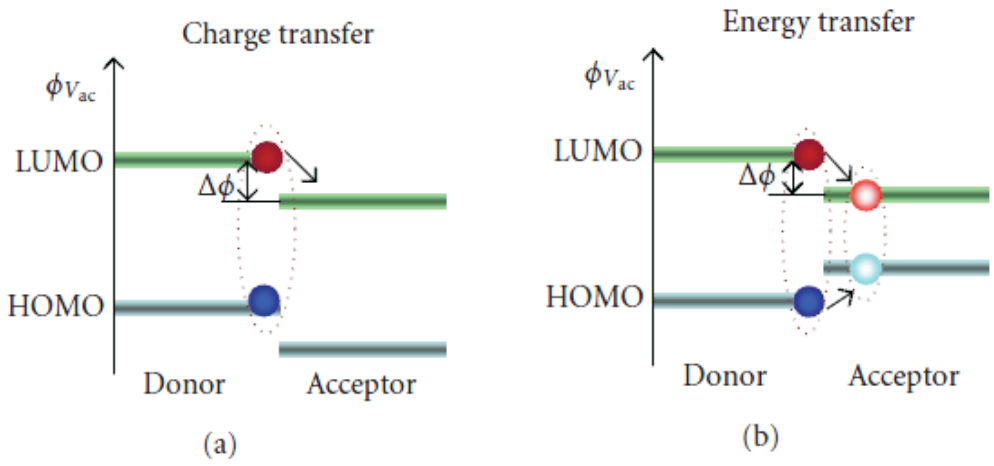

Figure 1.13: (a) Exciton dissociation via charge transfer, if the LUMO level offset between the donor and acceptor is larger than exciton binding energy. (b) If both the HOMO and LUMO of the electron acceptor are located between the HOMO/LUMO of the donor, energy transfer takes place.

This photoinduced charge separation process is also called 'photo-doping', since it is a photoinduced (in contrast to chemical or thermal induced) redox reaction between the donor and acceptor. In an organic bulk-heterojunction solar cell, the photons are absorbed by the donor or the acceptor, or by both. If the donor absorbs most of the incident light, the excitons are generated on the donor moieties. The process of photoexcitation, exciton decay, charge separation and recombination is explained below. Fig 1.14 demonstrates the loss mechanisms from the step of light absorption to the flowing photocurrent **[38]**. Upon light absorption, the excitons are generated. The excitons decay either radiatively (leading to photoluminescence) or non-radiatively through geminate recombination.

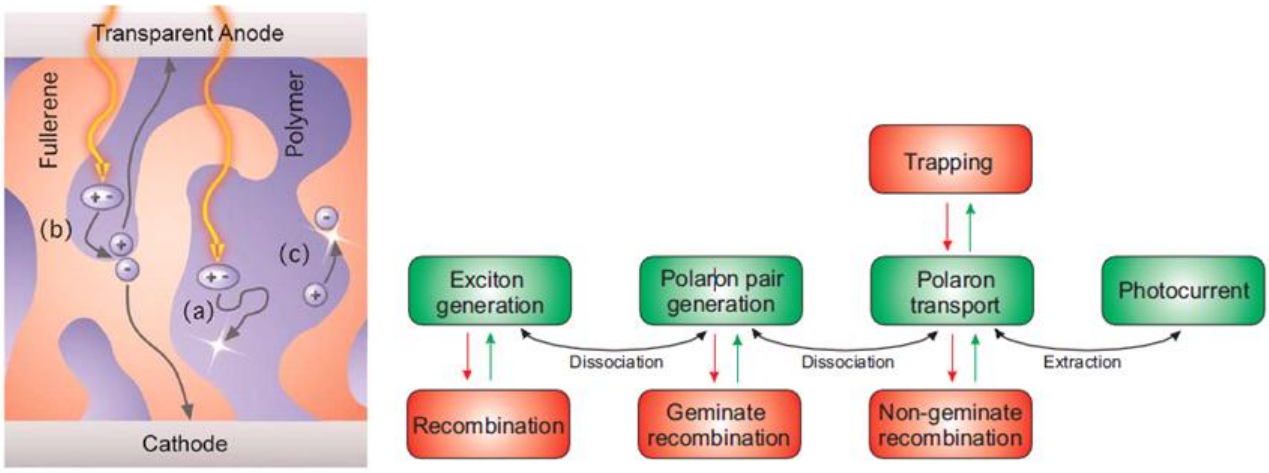

(a) **(b)**

Figure1.14: (a) The steps from light absorption to the flow of photocurrent in a polymer solar cell, and some loss mechanisms: process (a) corresponds to the photoluminescence due to excitons not reaching the donor–acceptor interface during their lifetime; process (b) corresponds to the polaron pair dissociation or geminate recombination of bound electron-hole pairs, respectively; and process (c) corresponds to the bimolecular recombination of free charge carriers. (b) For a high performance solar, the loss mechanism (red) have to be minimized for all steps.

If the excitons do not reach a D/A interface within their lifetime, they will recombine radiatively (process (a)), sending out photoluminescence. When the excitons reach the D/A interface, an electron transfer to the acceptor molecular yields a polaron pair (process (b)) where the geminate recombination could also happen (polaron pairs are the intermediate step from an exciton to a pair of free polarons). It should be noted that, under light illumination, some percentage of absorbed photons creates excitons, while the remaining percentage create spatially-indirect excitons, also referred to as neutral bipolarons (polaron pairs bound by Coulomb attraction). The geminate recombination of the neutral bipolarons is predominantly nonradiative. On the way of the separated charge carriers to their respective electrodes, charges can be trapped, or bimolecular recombination (process (c)) can take place **[38]**.

1.3.4 Charge Transport

After photoinduced electron transfer at the D/A interface and subsequent dissociation, the electrons are localized in the acceptor phase whereas the holes remain in the donor phase. Then, the free charge carriers must be transported via percolated pathways towards the electrodes to produce the photocurrent.

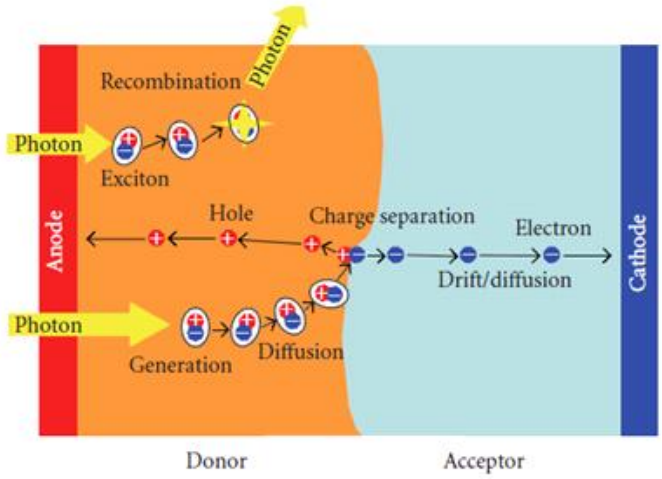

Figure 1.15: Principle of charge transport in a solar cell

If donor and acceptor phases are perfectly 'bicontinuous' between the two electrodes, and all LUMO and HOMO orbitals are nicely matched, the carriers would be able to diffuse smoothly towards their respective electrodes. Except for the influence of phase separation and pathways properties, the instinct characteristics of charge carriers, i.e., charge carrier mobility μ, also plays a critical role in determining the fluency and efficiency of charge transport in the device.

1.3.5 Extraction of the Charge Carriers at the Electrodes

In order to extract the photogenerated charge carriers via drift selectively to the respective electrodes, an energetically asymmetric structure is essential for an efficient solar cell. The difference of the work functions of the two electrodes induces a built-in electrical field, which causes a preferred direction for the charge transfer **[39]**. As transparent electrode, a layer of indium tin oxide (ITO) is used, and the selectivity of this electrode is usually enhanced by depositing a PEDOT: PSS (poly(3,4-ethylendioxythiophene)-polystyrene-para-sulfonic acid) layer on top. This PEDOT:PSS layer improves the surface quality of the ITO

electrode (reducing the probability of shorts) as well as facilitates the hole injection/extraction. PEDOT:PSS is generally applied as a dispersion of gelled particles in water. The highly conductive PEDOT:PSS layer can be obtained by spreading the dispersion on the ITO surface usually by spin-coating and driving out the water by heat. It is believed that for the efficient carrier collection at the electrodes, it is preferable when the acceptor LUMO level is close to the Fermi level of the small work function electrode (metals, such as aluminum) and the donor HOMO level is close to the Fermi level of the large work function electrode.

1.4. Characteristics of organic photovoltaic devices

Solar cells are characterised by measuring the current-voltage (*I*-*V*) curve under light illumination and dark. A typical current voltage (*I*-*V*) curve of a polymer solar cell is shown in Fig. 1.16. Since organic semiconductors show very low intrinsic carrier concentration, the metal-insulator-metal (MIM) model seems to be best suited to explain this characteristic. The characteristic points used to characterise a solar cell are labelled in Fig 1.16. In addition, for each of these points, the energy diagram for a single-layer cell with an indium tin oxide (ITO) anode and aluminium cathode is displayed. The point (a) on the curve corresponds to the current delivered by a solar cell under zero bias and is called short circuit current (Isc). In this case, excitons dissociation and charge transport is driven by the so-called built-in potential. In the MIM picture, this potential is equal to the difference in work function (Wf) of the hole and electron-collecting electrodes. For polymer solar cells, the transparent ITO (Wf, = 4.7 eV) electrode is often chosen in combination with a low work function Al (Wf, = 4.24 eV) **[40]** as counter-electrode to achieve a high internal field **[41,42]**. Point (b) on the curve shows the voltage where the current equals zero is called open circuit voltage (*V*oc). In the MIM picture this situation is described by the case where the band is flat, since the applied voltage equals the difference in the work function of the electrodes. Point (c) on the curve is for $V > V$oc, the diode is biased in the forward direction. Electrons are now injected from the low work function electrode into the LUMO and holes from the high work function electrode into the HOMO of the organic layer, respectively. Point (d) on the curve is for $V < 0$, and the diode is driven under a reverse biased condition the solar cells works as a photodiode. The field is higher than that at (a) which often leads to enhanced charge generation and/or collection efficiency.

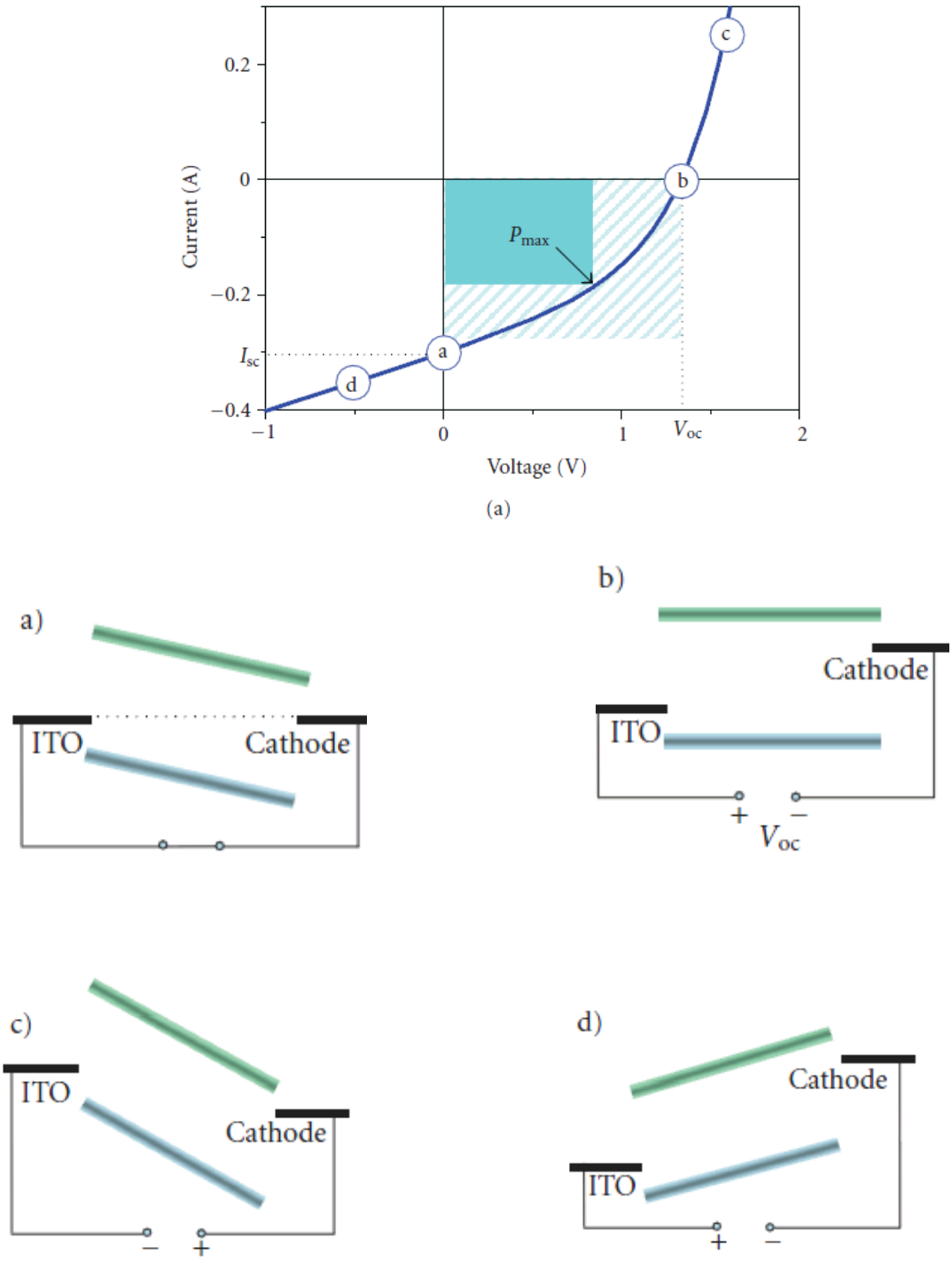

Figure 1.16: Current (voltage) characteristics of a typical organic diode shown together with the metal-insulator-metal (MIM) picture for the characteristic points. (a) Short circuit condition. (b) Open circuit condition. (c) Forward bias. (d) Reverse bias.

The spectral photocurrent efficiency commonly referred to as IPCE is calculated as the number of collected electrons per incident photon under short circuit condition.

$$IPCE = \frac{h \times c \times I_{sc}}{e \times \lambda \times P_{light}}$$

Here, λ is the incident wavelength, e the elementary charge, h the Planck constant, c the speed of light and P_{light} is the incident light power. The point where the electrical power $P = I \times V$ reaches the maximum value represents the condition where the solar cell can deliver its maximum power to an external load. It is called the maximum power point. The ratio of this maximum electrical power P_{max} to the product of the short circuit current and the open circuit voltage is termed the fill factor (FF):

$$\mathrm{FF} = \frac{P_{\max}}{I_{\mathrm{sc}} \times V_{\mathrm{oc}}}.$$

The ECE is defined as the ratio of the maximum electric power output of the cell to the incident optical power.

$$\eta = \frac{I_{\mathrm{sc}} \times V_{\mathrm{oc}} \times \mathrm{FF}}{P_{\mathrm{light}}}$$

CHAPTER 2

MATERIALS AND EXPERIMENTAL TECHNIQUES USED

2.0 Cell structure

2.0.1 Geometry

The polymer solar cells investigated in this theis have the layer structure ITO/PEDOT:PSS/P3HT:PCBM/Al,ITO/P3HT:PCBM/Al and PEDOT:PSS/P3HT:PCBM/Al. The methods spin coating and thermal evaporation were used for production of different layers. The cells are based on normal cell geometry. In normal geometry the transparent ITO electrode functions as the anode (hole collector) and the back metal Al electrode functions as the cathode (electron collecting).

2.0.2 The Active Layer

The active layer is where the photo-generation of charge carriers and charge separation takes place. It consists, as mentioned, of a BHJ comprising a donor and an acceptor material. P3HT is one of the most used semiconducting polymers in organic solar cells and cells based on P3HT generally have high efficiency and stability **[43]**. Regioregular P3HT is based on thiophene units joined at the 2 and 5 positions in a head-to-tail geometry, (Fig. 2.1 (a)). To be able to dissolve the thiophene a hexyl site group is added in the third position.

(a) **(b)**

Figure 2.1: Chemical structure of (a) the donor polymer P3HT (b) the acceptor PCBM

In solid state P3HT is semi crystalline and it has its maximum absorption around 500 nm **[44]**. Similar to other typical semiconducting polymers P3HT is hole conducting polymer due to its electron rich structure and high-energy HOMO level **[44]**. Organic materials with a high electron affinity are rare and the choice of acceptor materials is therefore limited **[44]**. The main material used in this thesis as acceptor is phenyl [6,6]- C61-butyric acid methyl ester (PCBM) - a soluble C60 based compound (Fig. 2.1(b)) . The electron mobility is on order of $2 \cdot 10^{-7}$ $m^2 \cdot V^{-1} \cdot s^{-1}$ and is therefore very useful as acceptor material. PCBM forms crystalline domains in the BHJ with P3HT and it actually increases the hole mobility of the polymer, even though the mechanism for this is not clear. Together, P3HT and PCBM is one of the most investigated combinations for the active layer and have large potential for high efficiency polymer solar cells.

2.0.3 Electrodes materials

In organic devices the work function of the electrode materials is very important since it determines together with the LUMO/HOMO and Fermi level of the semiconductor whether the electrode forms an ohmic or a blocking contact for the respective charge carrier (holes in VB, electrons in CB). Moreover a large difference in work function of the electrode materials can increase the V_{oc} considerably. The normal solar cell has two electrodes that ensure the electrical contact to the external circuit -the hole collecting anode and an electron collecting cathode. The front electrode needs to be transparent in order to let light through to the active layer. The back electrode is mostly based on a metallic non-transparent material.

Particularly Indium Tin Oxide (ITO) which is a degenerated semiconductor comprising a mixture of In_2O_3 (90%) and SnO_2 (10%) with a band gap of 3.7 eV and a Fermi-level between 4.5 and 4.9 eV is used. The large band gap allows no absorption of wavelengths longer than about 350 nm. ITO is the most used transparent electrode for organic electronic devices. It is transparent over a broad range of wavelengths and has a high electrical conductivity with current densities of 5-10 $mA \cdot cm^{-2}$ and sheet resistivity of 4-8 $\Omega \cdot sq^{-1}$. In the inverted cell construction ITO function as is the electron collecting electrode. The work function of ITO varies with treatment, and interface layers such as PEDOT:PSS or Zinc oxide (depending on the flow of current) is therefore added in between ITO and active layer. In this project we used metallic back electrode Al, processed via high-vacuum thermal evaporation.

2.0.4 Buffer Layers

The charge carrier transport at the interface between the organic materials and electrode is difficult. In order to improve this, a widely used solution is to introduce as a thin layer, called buffer layer, which have several functions. It adjusts the electronic behaviour of adjacent materials, it protects the organic layer from the diffusion of electrode material, and obstruct the permeation of oxygen and water molecules. It is therefore necessary to incorporate a buffer layer, which reduces the barrier between hole collecting electrode and the active layer **[45]**. Poly-(ethylenedioxythiophene):polystyrensulphonic acid (PEDOT-PSS), which is a hole transporting layer, is therefore sandwiched between the active layer and the anode. It smoothes its surface and enhance the adhesion of organic onto ITO substrate. The water soluble PETDOT:PSS ensures better transportation of holes by increasing the stability of the electrical contact. PEDOT-PSS is a molecularly doped conjugated polymer, (see Fig. 2.2) with a higher work function than ITO. It is semitransparent with a light blue color **[46]**.

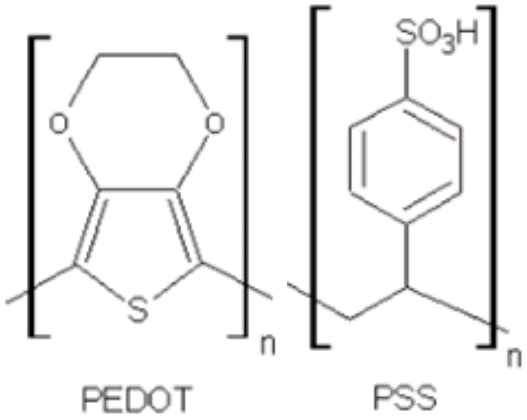

Figure 2.2: Chemical structure of the donor polymer PEDOT and the acceptor PSS

Regarding conductivity, PEDOT:PSS can achieve performance in the same order of magnitude as metals **[46]**. PEDOT:PSS does also improve the surface roughness of the active layer. The main drawback of PEDOT:PSS is its degradation in open atmosphere. Due to highly hygroscopic nature of PEDOT:PSS it introduces water into the organic films which becomes a main source of degradation in organic solar cell.

2.1 Experimental Techniques used

2.1.1 Standard glove box

To make the devices in inert atmosphere we used a glove box. Fig. 2.3 shows the photograph of the glove box at NPL, New Delhi. There are two gloves arranged in such a way that the user can place his or her hands into the gloves and perform tasks inside the box without breaking the seal or allowing potential injury. Part or all of the box is usually transparent to allow the user to see what is being done inside. Two types of glove boxes exist: one allows a person to work with hazardous substances, such as radioactive materials or infectious disease agents; the other allows manipulation of substances that must be contained within a very high purity inert atmosphere, such as argon or nitrogen. It is also possible to use a glove box for manipulation of items in a vacuum chamber. During the use of glove box first we load the samples into antechamber in following steps.

Transferring the materials into antechamber

1. Make sure that the antechamber is currently "under vacuum".

2. Back fill antechamber and open the gate of antechamber.

3. Load the materials into the antechamber and then evacuate and refill the antechamber for at least three times.

Transferring the materials from antechamber to glove box

1. Make sure that both the refill valve and evacuation valve are closed.
2. Insert hands & arms into the black rubber gloves while using the left side of the foot pedal to decrease pressure within the box.
3. With hands inside black rubber gloves, open the inner door handle and then swing door upward to open.
4. Move items in or out of the chamber.
5. Check the door seal for any debris, and then swing the door back down and close the door of antechamber. Evacuate the antechamber at working time.

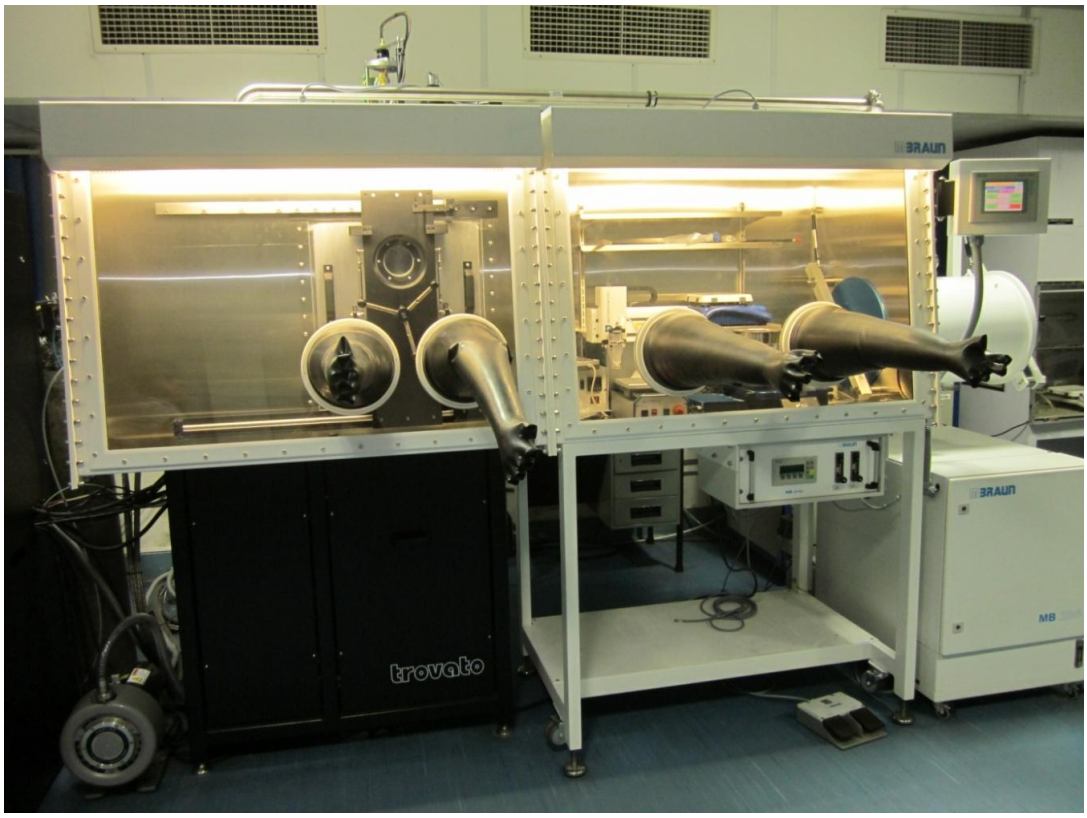

Figure 2.3: Glove box at NPL, New Delhi

In glove box, we can use different types technique as spin coating, encapsulation, annealing etc. After coating the active layer, we can deposit the top electrode by thermal evaporation technique by transferring the sample in thermal evaporation chamber which is also connected to glove box. After making the devices we refill the antechamber and open the gate of anti chamber to unload the devices. Spin coating and Thermal evaporation technique used in our lab are described below.

2.1.2 Spin Coating technique

Spin coating is the most widely used deposition technique so far for the development of organic solar cells. Highly reproducible as well as very homogenous films can be deposited by this technique. In principle, its operation can be described as: an excess amount of a solution is introduced on the substrate which is going to be accelerated to a chosen rotational speed in order to spread the fluid by centrifugal force. Fig. 2.4 shows the basic principle of spin coating process. The angular velocity of substrate with the overlying solution gives rise to the ejection of most applied solution and only a thin film remains on the substrate. Using spin coating technique the thickness, morphology and surface topography of

the final film obtained from a particular material in a given solvent and at a given concentration is highly reproducible. Fig. 2.5 shows the photograph of spin coater used in the present project.

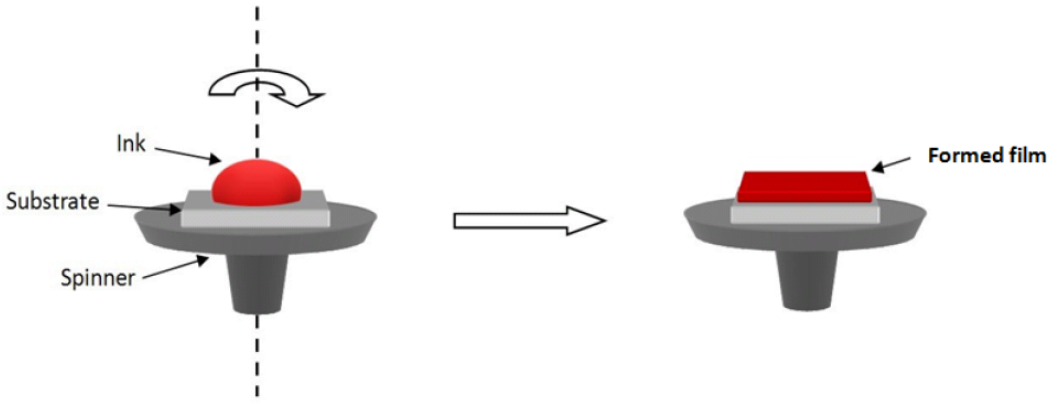

Figure 2.4: Schematic illustration of the spin coating technique

It has been commonly acknowledged that the spin coating technique is an excellent experimental technique on a laboratory scale. However, for commercialization of the OPV technology, where mass and large-scale production is required, spin coating becomes uncompetitive. In our lab we used digital spin coater in which time and speed can be set according to the need. To hold the sample rotary pump is used, which is connected to spin coater, so there is no chance for the sample to fell down while spinning. Millipore 0.4 μm filters were used to filter the PEDOT:PSS before deposition.

Figure 2.5: Digital spin coater used in lab NPL, New Delhi

2.1.3. Thermal evaporation

Thermal evaporation is a widely used method to deposit metal films. The source material is evaporated at high temperature and vacuum, and the ejected atoms travel directly to the substrate where they condense back to a solid state. Fig. 2.6 shows schematically the working and thin film preparation in a vacuum chamber via thermal evaporation of the depositing materials.

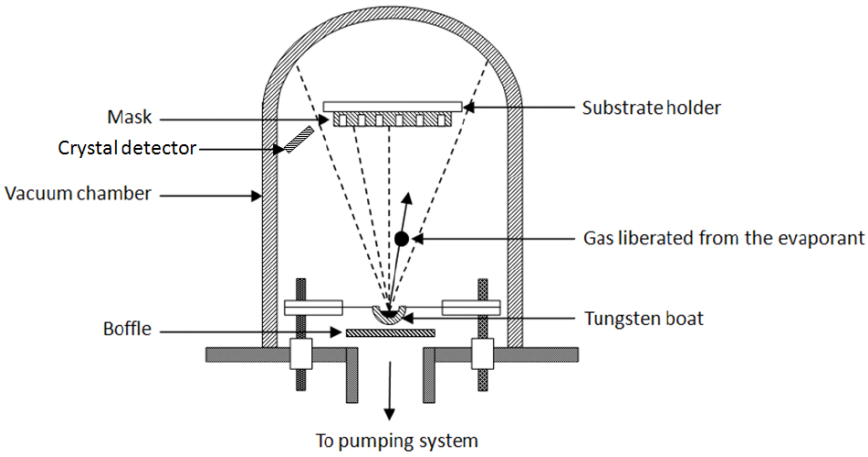

Figure 2.6: Working of thermal evaporation system

Fig. 2.7 shows the photographs of the thermal evaporators used at NPL and used in this project. Vacuum is usually required to remove vapours other than the source material before the evaporation begins, because evaporated atoms may never reach the substrate, if they collide with other foreign atoms too frequently, and furthermore, the collision may cause the

evaporated material to react with foreign atoms. For instance, if aluminium is deposited in the presence of oxygen, it will form aluminium oxide instead of pure aluminium. So for aluminium deposition high vacuum is required.

(a) **(b)**

Fig. 2.7 (a): Thermal evaporation unit and, (b). Thermal evaporation unit connected with glove box in NPL

2.1.4. Work function determination of the PEDOT:PSS layer

We made the electrodes of PEDOT:PSS layer of different thickness and calculated their work function with respect to their thickness. The work function (Wf) is the least amount of energy required to remove an electron from the surface of a conducting material, to a point just outside the metal with zero kinetic energy. As the electron has to move through the surface region, it's energy is influenced by the chemical, optical, electric and mechanical characteristics of the region. Hence the workfunction is an extremely sensitive indicator of surface condition and is affected by absorbed or evaporated layers, surface reconstruction, surface charging, oxide layer imperfections, surface and bulk contamination, etc. To calculate the work function we used the **UHV KELVIN PROBE** instrument. It is a non-contact, non-destructive vibrating capacitor device used to measure the work function difference, or for non-metals, the surface potential, between a conducting specimen and a vibrating tip. The Kelvin method was first postulated by the renowned Scottish scientist W. Thomson and later by Lord Kelvin, in 1861. Fig. 2.8 shows the Kelvin probe head and the tip preamplifier which is connected with the Digital control unit.

Fig. 2.8: UHV Kelvin probe head unit (right). The tip preamplifier is contained within the external and Digital Control Unit Front Panel (left).

2.1.5 Determination of the active layer thickness (P3HT:PCBM) and PEDOT:PSS layers:

To measure the thickness of different PEDOT:PSS layer we used the Ellipsometer. An Ellipsometer enables to measure the refractive index and the thickness of semi-transparent thin films. An Ellipsometer measures the changes in the polarization state of light when it is reflected from a sample. If the sample undergoes a change, for example a thin film on the surface changes its thickness, then its reflection properties will also change. Measuring these changes in the reflection properties can allow us to deduce the actual change in the film's thickness. The most important application of Ellipsometry is to study thin films. Fig. 2.9 shows the photograph of Ellipsometer used for thickness determination in the present proposal.

Figure 2.9: Ellipsometer used for thickness of PEDOT:PSS layer, NPL

In the context of Ellipsometry a thin film is one that ranges from essentially zero thickness to several thousand Angstroms, If a film is thin enough that it shows an interference color then it will probably be a good Ellipsometric sample. The sensitivity of an Ellipsometer is such

that a change if film thickness of a few Angstroms is usually easy to detect.

2.1.5. Transmission determination of PEDOT:PSS layer

To check the transmission of different thickness of PEDOT:PSS layer we used **UV-VIS SPECTROPHOTOMETER**, which has the range up to 300 nm to 1100 nm. Transmission Spectroscopy is highly interrelated to Absorption Spectroscopy. This technique can be used for solid or liquid, samples. Here, light is passed through the sample and compared to light that has not been incident called reference light. The output depends on the path length or sample thickness, the absorption coefficient of the sample, the reflectivity of the sample, the angle of incidence, the polarization of the incident radiation, and, for particulate matter, on particle size and orientation.

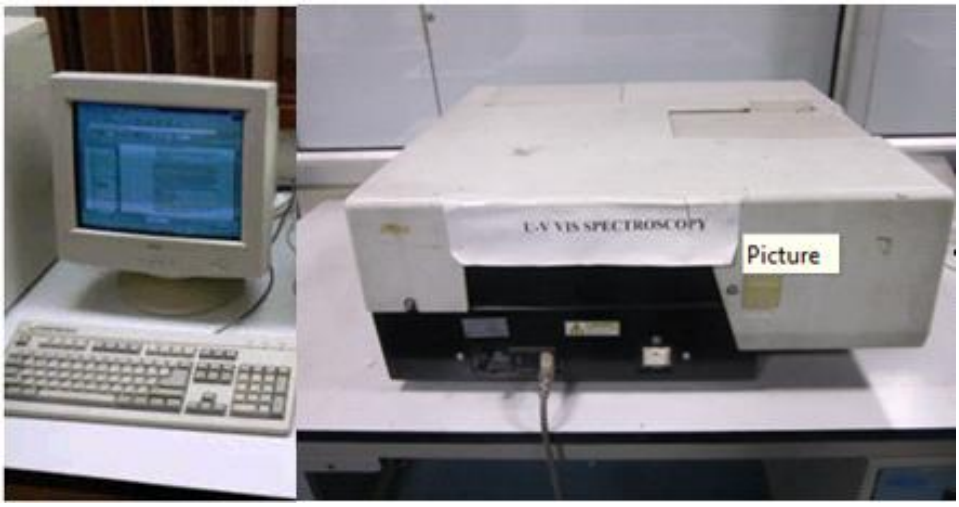

Figure 2.10: UV-VIS SPECTROPHOTOMETER at NPL, New Delhi

According to Beer Lambert Law the term I_T/I_o is called transmittance, where I_T is the monochromatic radiant power transmitted by the absorbing medium and I_o is the monochromatic radiant power incident on the medium. This form of spectroscopy has a setup similar to the one used for Absorption.

Chapter 3
Fabrication of Organic Solar cells

3.1 Cleaning and pre-treatment of ITO substrates

In this thesis, glass substrates coated with 100 nm of indium tin oxide (ITO) were used as the transparent electrode. The glass substrates had a square shape of 2.5×2.5 cm^2. In order to achieve the bottom electrode, the substrate was first covered with tape, which was cut into desired geometry and shape. Now the removal of unwanted tape and exposure to a HCl+Zinc dust solution for 2 min resulted the etching and patterning of ITO into desired structure. The structured ITO substrates were washed with plenty of water right after etching. For cleaning step, the substrates were placed in a glass sample holder filled with the washing solvent and the sample holder was placed in an ultrasonic bath (Fig 3.1(a)) for 20 minutes. Afterwards, the washing solution was first poured away and the substrates were then rinsed with distil water to ensure that no organic solvent remained on the sample surface and again placed in ultrasonic bath.

(a) **(b)**

Figure 3.1(a): Sonicator with glass holder and (b) Hot plate used for ITO cleaning, at NPL .

After that these substrates were subsequently (Fig 3.1(b)) boiled in acetone, trichloroethylene and propanol respectively by puting on to a hot plate for 10 minutes each and dried in vacuum oven at 120^{o}c for 20 minutes (Fig. 3.2 (a)). A 50 nm thick conductive polymer polystyrene sulfonic acid doped poly(3,4- ethylenedioxythiophene) (PEDOT:PSS) (Aldrich Chemicals, 1.3 wt % dispersion in water) was spin-coated on the patterned ITO

substrate to reduce the surface roughness. PEDOT:PSS is a hole-transporting polymer and has work function of 5.1 eV about 0.3 eV higher than that of ITO (4.8 eV). This leads to a reduction in the injection barrier between ITO and active layer. Before the spin-coating of PEDOT:PSS, oxygen plasma treatment was applied for 5 minutes (Fig 3.2(b)) to the ITO substrates to ensure that no impurities were attached to the surface and to make the ITO surface more hydrophilic, allowing better wetting with the conductive polymer layer.

(a) (b)

Figure 3.2(a): Vacuum oven and (b) Plasma cleaning of ITO, at NPL

After the deposition of PEDOT:PSS layer these substrate were placed in vacuum oven (Fig. 3.2(a)) at 120^{o} C to evaporate the solvent and curing of PEDOT:PSS film.

3.2 PEDOT:PSS electrode in ITO free solar cell

For making the PEDOT:PSS electrode as a anode, we take the plane glass substrates having a square shape of 2.5×2.5 cm^2.These glass substrates were cleaned in identical manner as ITO substrates. Then PEDOT:PSS was spin-coated on the entire substrate with different speed 1000, 2000 and 3000 rpm for 1 min. to get the different thickness. After that we used Teflon tape and cut the tape into the form of desired electrode then we covered the substrate by these strips and removed the uncovered area with the help of water. After removing the uncovered area we removed the strips and got the electrode of PEDOT:PSS. There is no problem in removing the uncovered area with water because water is used as a solvent for

PEDOT:PSS and there is no chance for adhesion of particle from the Teflon tape. After making these electrodes these substrate were transferred to vacuum oven for annealing.

3.3 Deposition of the active organic layer

Solution deposition: For the polymer blend (P3HT:PCBM), P3HT (purchased from Aldrich Chemicals, USA) and PCBM (purchased from Nano-C, USA) were dissolved in a suitable solvent. In this project we used chlorobenzene as a solvent for (P3HT:PCBM blend) and then this solution was ultrasonicated for 30 min to form a homogeneous solution. The concentration of P3HT:PCBM were changed to optimized the cell performance.

Figure 3.3: Weigh instrument and sample hold in sonicator

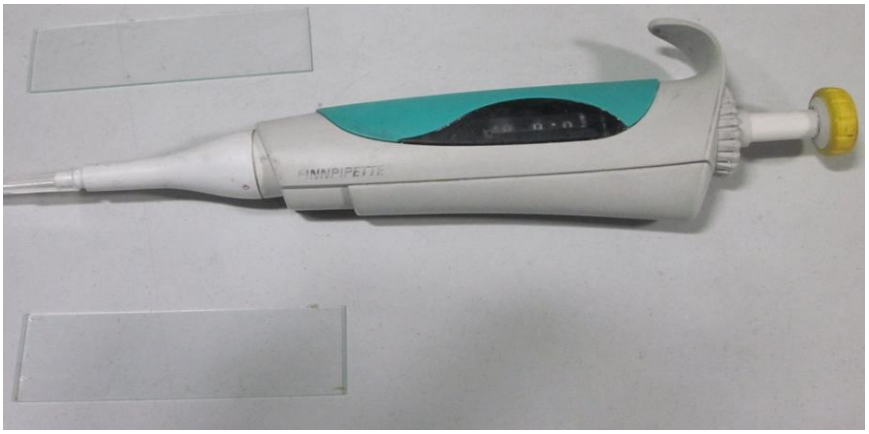

Figure 3.4: Micropipette used for dropping the solution onto substrate

After that these substrates were transferred into glove box. Polymer film spin coating was done by taking the solution with a micropipette and immediately dropping the solution

onto the substrates. The spin coater was started directly after dropping the solution, rotation time and speed was set according to the experimental needs. Then these substrate were placed onto a hot plate with constant temperature. These polymer films were annealed at 120 ^{0}c for 30 minutes in glove box under a nitrogen atmosphere at 10^{-1} mbar.

3.4 Top electrode evaporation

After the solution (P3HT:PCBM) deposition of the active organic layer, the samples were transferred into the metal evaporation chamber, where the top electrode materials were thermally deposited directly onto the active layer through a metal mask. By placing the masks properly with respect to the etched ITO stripes, 4 individual pixels with the active area of each cell defined by the cross section of the top electrode and the ITO stripe, here typically between 0.065 and 0.09 cm^2, were formed. The top electrode material used in this project is aluminium (Al). Suitable amounts of the metals were placed in the source boat, on the lower part of the evaporation chamber. The boats were made by tungsten wire and used after flashing.

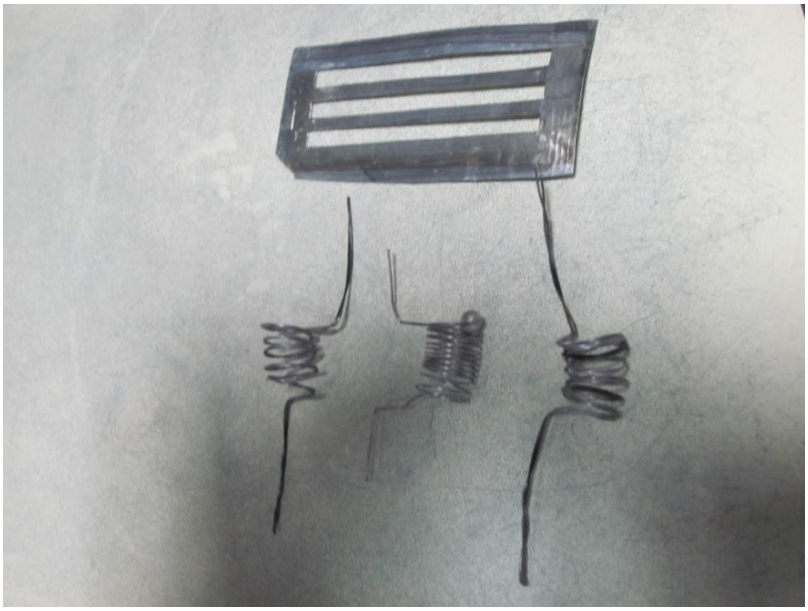

Figure 3.5: Tungsten boat and Metal mask used in Al deposition

The chamber was then closed after closing the source shutter and the sample shutter. Vacuum was applied and the evaporation started when the pressure reached 2×10^{-6} mbar.

Since the metal source position is fixed, the sample plate was to rotate slowly to obtain a homogeneous film. The current through the boot was regulated to keep the evaporation rate constant. The source shutter and sample shutter were opened when the metal started to evaporate and when the evaporation rate became constant. For the solar cell a 100 nm Al layer was deposited as a top electrode. After the evaporation step, the devices were placed on hot plate at 150^0C for 6 minutes for post production (annealing) treatment.

3.5 Photovoltaic Characterization

After making the devices these devices were held in open atmosphere for degradation measurements either in the dark or exposed to illumination light. Light was generated from tungsten halogen lamp from Osram, Germany, with the help of home made setup, to illuminate the cells at 100 mW/cm^2. The current density-voltage (*J-V*) characteristics of the samples were recorded using Keithley 2420 SourceMeter unit interfaced with computer.

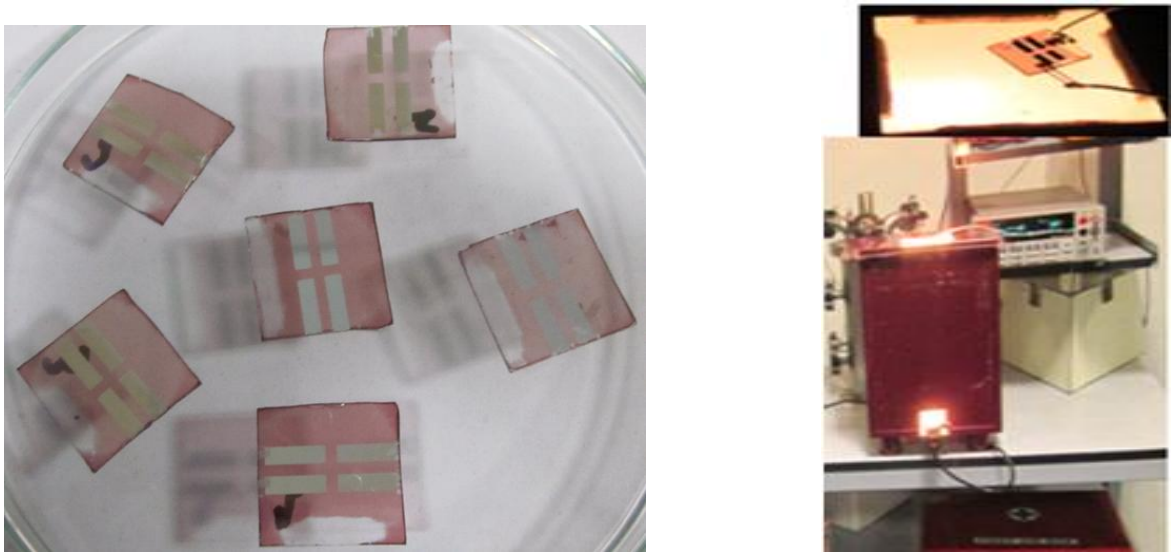

(a) **(b)**

Figure 3.6(a): Images of devices ready for characterization in which the side area was uncovered for making the contact for ITO and (b) The setup kiethley source meter 2420 ,used for characterization at NPL, Delhi

The sample was placed on a measurement-box and two contacts were made, one for ITO and the other for Al electrodes. The photovoltaic cell characteristics, namely the open circuit voltage (V_{OC}), short circuit current density (J_{SC}), fill factor (FF) and power conversion efficiency (η), were measured under illumination and dark in ambient condition.

Chapter 4
Result and Discussion

4.0 Optimization of Materials

First of all we optimized the materials concentration of blend used for active layer to get the better performance for investigations in better devices. We take the different concentration of (P3HT:PCBM blend) material for active layer. Photovoltaic (PV) devices were fabricated on pre-clean patterned ITO glass substrates. A few nm hole extraction layer of PEDOT:PSS was applied onto the substrates by spin coating. The PEDOT:PSS film was annealed at 120ºC for 30min. On top of the PEDOT:PSS the active layer of P3HT:PCBM was deposited. P3HT:PCBM blends were prepared at four different donor-acceptor ratios (1:0.5), (1:0.08), (1:1) and (1:1.5) in chlorobenzene solution. The blends were then left in ultrasonic bath for 30 minutes.

The solutions were deposited by spin coating with a speed of 2000 rpm for 1 minute and dried on the hot plate at 120ºC for 30 minutes. The layers thicknesses of the blends were around 155 nm. Finally, the substrates were then loaded into a thermal evaporator for the deposition of the cathode material, 100 nm Al layer was deposited through a metal mask a mask on top of the active layer under high vacuum. After this, the devices were annealed at 150 ºC during 6 min. Each substrate contained four solar cell devices with an active area of 9 mm^2. Fig. 4.1 shows the current density–voltage characteristics (J-V) of the devices measured under 100 mW/cm^2 in open atmosphere. Table 1 shows the performance of different devices. The variation in the performance of the solar cells with different donor-acceptor ration can be attributed to the change in the nano-scale morphology and different electronic properties of the blend. In P3HT:PCBM active layer the phase separation takes place and nano crystallites of P3HT and PCBM are formed. The size of the nano-crystallites depends on the wt% ratio of the constituents. The nano-scale morphology controls the current through the active layer and as a result the efficiency.

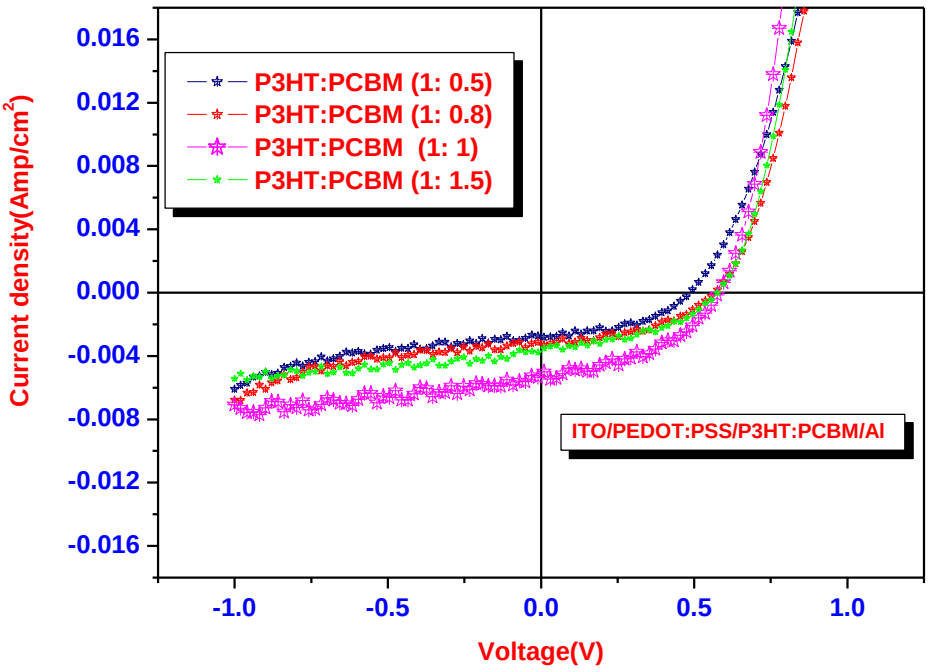

Figure 4.1: Illuminated J-V characteristics of the P3HT:PCBM solar cells with different donor-acceptor concentrations.

Table 1 Performance of the devices with different weight ratio of P3HT and PCBM

P3HT:PCBM wt (%)	J_{sc} (mA/cm^2)	V_{oc} (V)	FF (%)	η (%)
1:0.5	2.74	.47	49	.639
1:0.8	3.12	.56	50	.828
1:1	5.34	.58	52	1.43
1:1.5	3.76	.55	51	.91

It is clear from the table that the blend with the best performance was obtained for 1:1 donor-acceptor ratio which exhibits the power conversion efficiency (η) of 1.43 %, open circuit voltage (V_{oc}) of 0.59 V, short current circuit density (J_{sc}) of 5.34 mA/cm^2 and the fill factor (FF) of 52 %. Table 1 shows all the parameter extracted for all blends as prepared.

4.1 Degradation study in solar cell

In this section we analyse the role of ITO and PEDOT:PSS on stability and degradation of P3HT:PCBM bulk-heterojunction solar cells. For comparison point of view and to examine the role of PEDOT:PSS in the degradation of organic solar cells we did prepare solar cells with PEDOT:PSS only as anode (without ITO). For detailed investigations the devices were prepared in the following configurations: ITO/PEDOT:PSS/P3HT:PCBM/Al, ITO/P3HT:PCBM/Al and PEDOT:PSS/P3HT:PCBM/Al (wtihout ITO). The performance of these devices in terms of efficiency and degradation is discussed below.

4.1.1 Degradation in ITO/PEDOT:PSS/P3HT:PCBM/Al and ITO/P3HT:PCBM/Al devices

Fig. 4.2 Shows the *J-V* characteristics, of ITO/PEDOT:PSS/P3HT:PCBM/Al and ITO/P3HT:PCBM/Al devices measured under illumination just after preparation. The device ITO/PEDOT:PSS/P3HT:PCBM/Al exhibited J_{sc} of 5.14 mA/cm^2, V_{oc} of 0.58 V, FF of 48.6 % and η of 1.34 % and the device and ITO/P3HT:PCBM/Al exhibited J_{sc} of 2.78 mA/cm^2, V_{oc} of 0.55 V, FF of 45 % and η of 0.82 %.

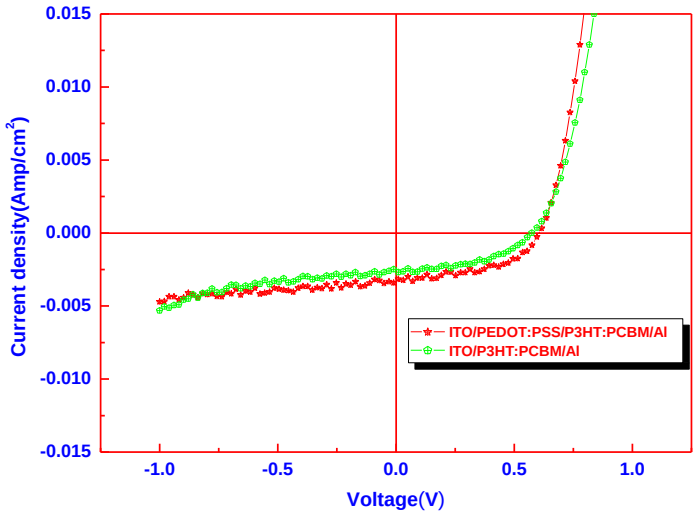

Figure 4.2: Illuminated J-V characteristics of the P3HT:PCBM solar cells with and without PEDOT:PSS for anode.

The photovoltaic characteristics of the devices were measured in the open atmosphere. It has been found that the devices with PEDOT:PSS shows the better performance in comparison to the devices without PEDOT:PSS. PEDOT:PSS provides a well-defined work function which is higher than that of ITO, it smoothes the rough ITO surface and so avoids shorts. But the devices with PEDOT:PSS shows the fast degradation in comparison to the devices with out PEDOT:PSS. Fig. 4.3 shows the variation of illuminated *J-V* characteristics of the devices with time. Device with PEDOT:PSS exhibited poorer stability compared to that without PEDOT:PSS. The fast degradation with PEDOT:PSS can be attributed to the hygroscopic nature of PEDOT:PSS. It absorbs water and losses its electronic properties, and as a result increases the resistivity of the device. It is well known that ITO is very sensitive to acid environments. Due to the strong acidic nature of PSS, the aqueous solution from which the PEDOT:PSS films are cast can also be expected to etch the ITO and changes its properties. Studies show that from ITO, In diffuses into active layer and up to Al electrode. The hygroscopic nature of PSS probably plays an important role. Upon exposure to air, water will be absorbed by the PEDOT:PSS film and an aqueous acid environment is formed due to the reaction H_2O + PSS (HSO_3)→ H_3O^+ + PSS(SO_3). This will facilitate etching of the ITO and transport of the etch products throughout the PEDOT:PSS film and up to the top Al electrode through active layer.

Fig 4.3 (b) shows that in initial stage of degradation the current density of the devices with PEDOT:PSS is faster as comparison to the devices without PEDOT:PSS. The degradation in open circuit voltage (V_{oc}) was also more in comparison to the devices without PEDOT:PSS but not as large as that in current density. The V_{oc} values of the devices will not depend only on the work functions values of the electrode but will depend also on the Fermi levels of polymer (P3HT) and fullerenes (PCBM). So the devices with PEDOT:PSS shows the fast degradation in current density comparison to the devices without PEDOT:PSS.

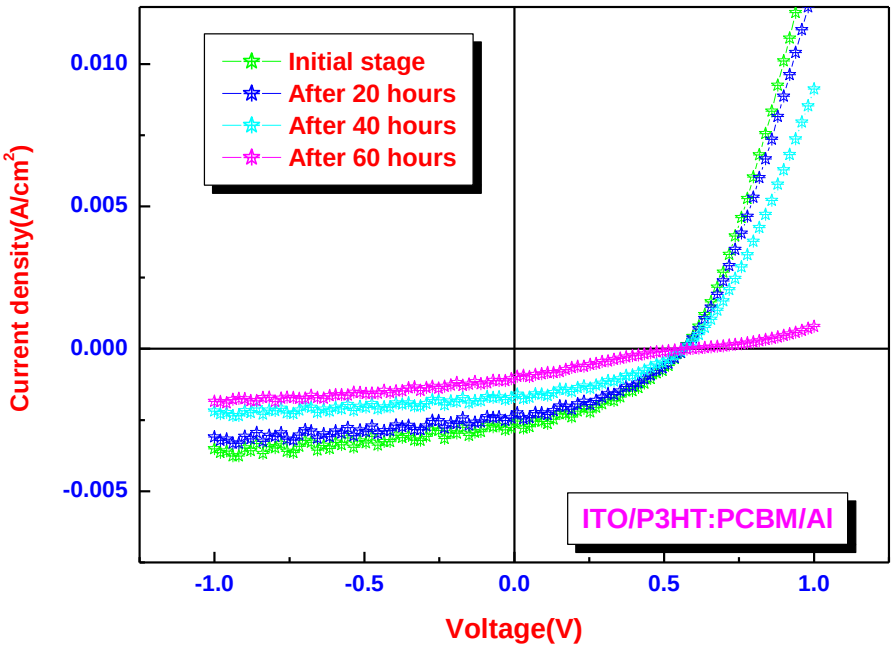

Figure 4.3(a): Variation in the illuminated J-V characteristics of ITO/P3HT:PCBM/Al cell with time.

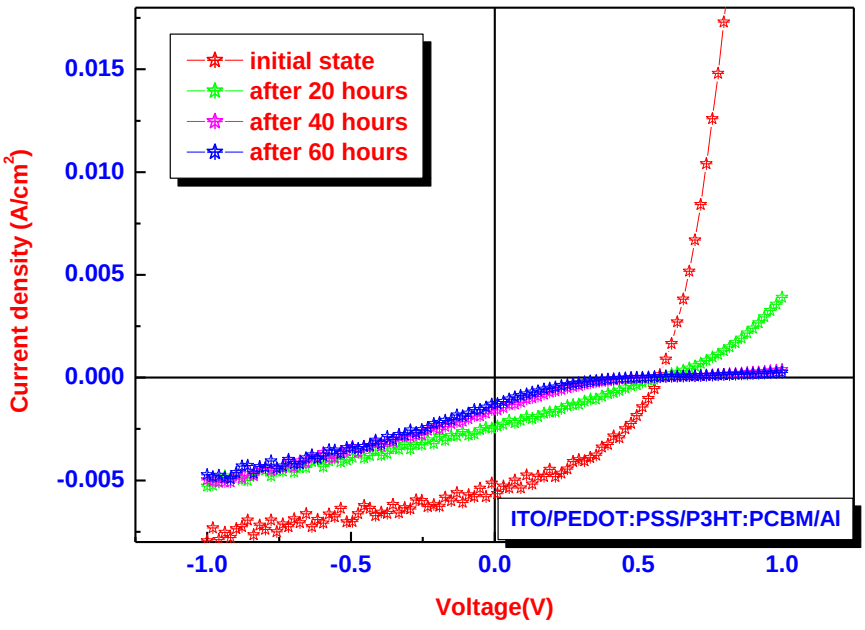

Figure 4.3(b): Variation in the illuminated J-V characteristics of ITO/PEDOT:PSS/P3HT:PCBM/Al cell with time.

4.2. Degradation in PEDOT:PSS/P3HT:PCBM/Al devices (ITO free solar cell)

Figure 4.4 (a) shows the current-voltage characteristics in dark and under illumination at 100 mW/cm^2 for PEDOT:PSS/P3HT:PCBM/Al devices without ITO. Fig. 4.4 (b) shows the variation in *J-V* characteristics of PEDOT:PSS/P3HT:PCBM/Al solar cells with time. Due to the high resistivity of PEDOT:PSS film the value current density (J_{sc}) is very small but the value of open circuit voltage (V_{oc}) is high due to the high work function of PEDOT:PSS which is greater then ITO. Decrease in J_{sc} of solar cell without ITO could be explained by the degradation of PEDOT:PSS film or increase in resistance in PEDOT:PSS film. PEDOT:PSS is hygroscopic in nature. It absorbs water from atmosphere and oxidizes fastly. Moisture and oxygen in air have a profound influence on the film degradation. The combined effects of moisture and oxygen should be taken into account when the effect of air is considered. For conducting polymers, the decrease in the conductivity in air at room temperature was ascribed to absorbed water while, at higher temperatures, both oxygen and moisture were considered to cause the degradation.

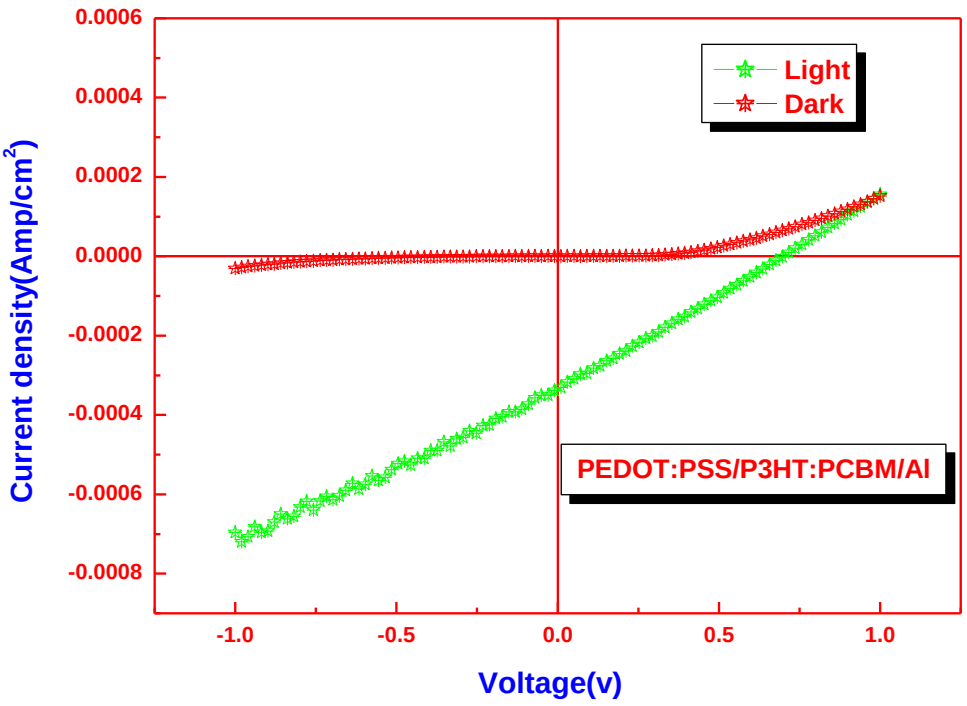

Fig. 4.4(a): Dark and illuminated J-V characteristics of PEDOT:PSS/P3HT:PCBM/Al solar cell

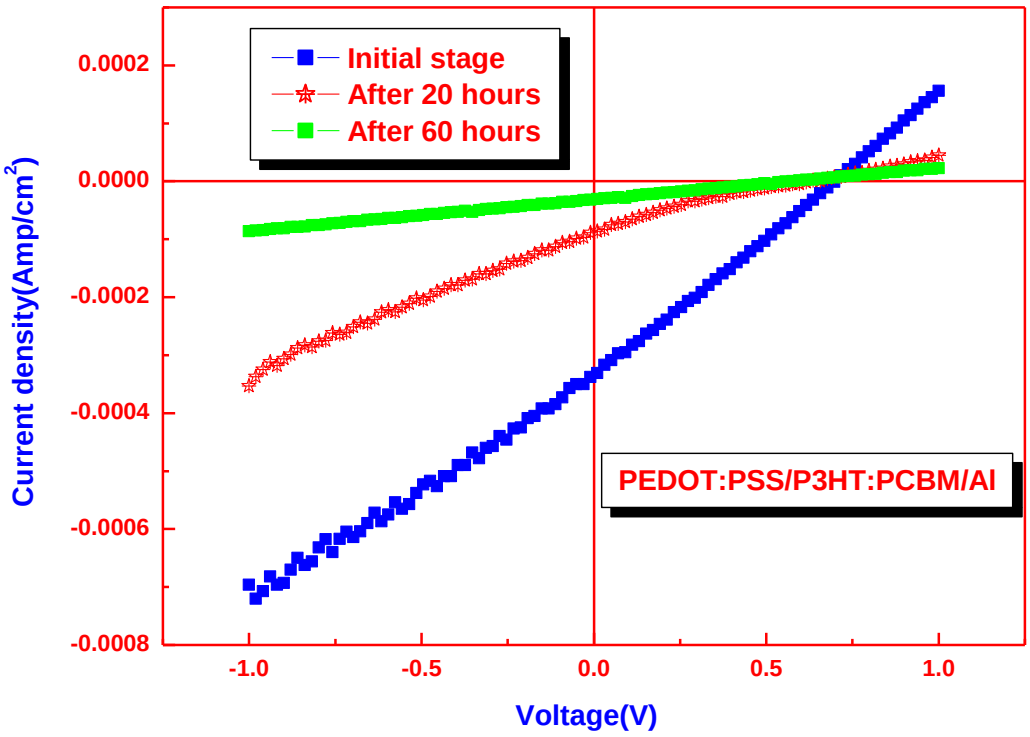

Figure 4.4(b): Variation in the illuminated J-V characteristics of PEDOT:PSS/P3HT:PCBM/Al solar cell with time.

Fig. 4.5 shows the I-V characteristic of PEDOT:PSS electrode on the plain glass with respect to time. By this figure we can analyse that as the time increases the current in PEDOT:PSS electrode decreases. These results confirms that resistivity of PEDOT:PSS layer increases with time in open atmosphere. So in open atmosphere there is degradation in PEDOT:PSS layer and it's resistivity will increase and the current density of the device decreases very fastly. The work function will also decrease because the work function of a surface is strongly affected by the condition of the surface. The presence even of small amounts of contamination (less than a monolayer of atoms or molecules), or the occurrence of surface reactions (oxidation or similar) can change the work function substantially. Changes of the order of 1 eV are common for metals and semiconductors, depending on the surface condition. These changes are the result of the formation of electric dipoles at the surface, which change the energy necessary for an electron to leave the sample.

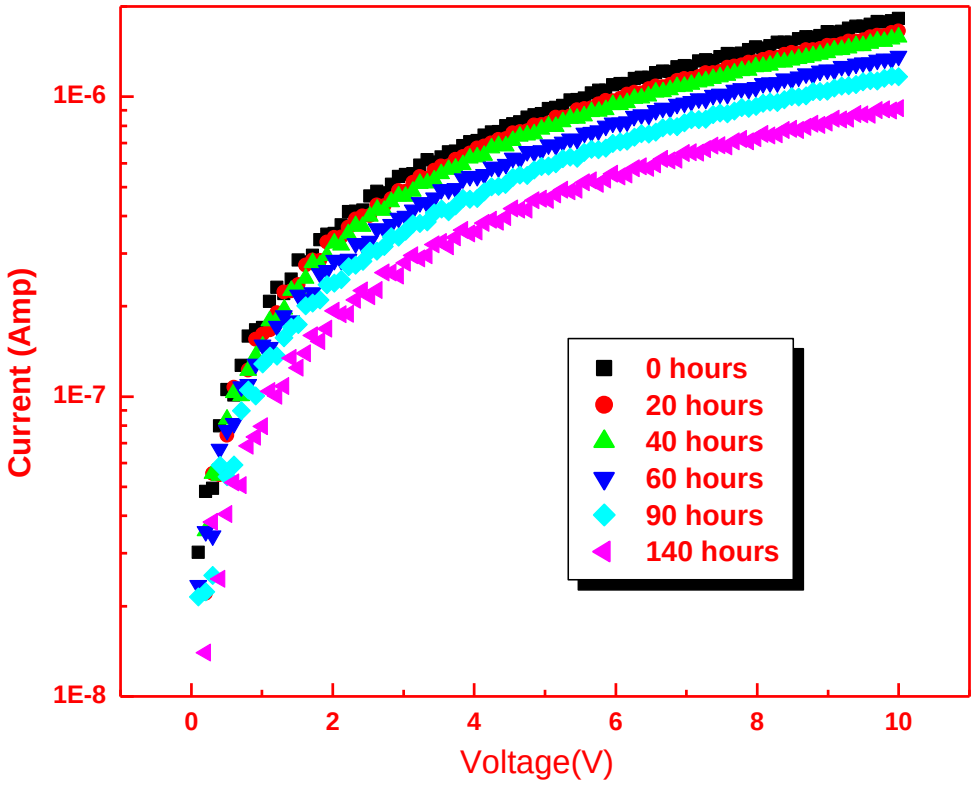

Figure 4.5: Variation in the current through PEDOT:PSS electrode with time

So when we studied the degradation of these devices in our lab we found that the current density of the device decreases very fastly and can be attributed to increase in the resistivity of PEDOT:PSS layer. It is important to remark that the cells keep their V_{oc} quite constant. As there was negligible variation in Voc with time in the present device, it can be attributed to the difference of HOMO of donor and LUMO of acceptor or the Fermi levels of polymers and fullerenes to be the dominant factor to control the Voc.

4.3 Effect of thickness PEDOT:PSS layer on the performance of polymer solar cell

To check the effect of thickness of PEDOT:PSS layer we made the ITO free solar cell (PEDOT:PSS/P3HT:PCBM/Al) with different thickness of PEDOT:PSS. Before making these cells we took the plain glass substrate (without ITO). Then these substrates were cleaned in identical manner as the ITO substrates for device fabrication. Then the hole conducting layer of PEDOT:PSS was spin coated on the top of glass substrates with different

spinning rates of 1000, 2000 and 3000 rpm respectively for 60 second and then dried in vacuum oven at 120^{o}C for 30 minutes. We measured the thickness of all PEDOT:PSS layers with the help of "ELLIPSOMETER". The thickness was found to be 180,150 and 90 nm for spinning rate 1000, 2000 and 3000 rpm respectively. After the measurement of thickness of the layers we calculate the work function of PEDOT:PSS layers of different thickness with the help of "UHV KELVIN PROBE" and we found that the work function of PEDOT:PSS increases with increases the thickness of layers. We also measured the transmission of these layers. Fig. 4.6 shows the transmission spectra of PEDOT:PSS layers of different thicknesses. In this figure we can see that as the thickness of PEDOT:PSS layer increases the transmission decreases . We did also measure the *I-V* characteristics of these layers.

Fig. 4.7 shows the I-V curves of different PEDOT:PSS layers with different thicknesses. It is seen that most thicker layer show highest current in comparison to other layers. It means that the conductivity of PEDOT:PSS layer increases as the thickness of layer increases. After taking these result we made the devices in PEDOT:PSS/P3HT:PCBM/Al configuration in identical manner as above.

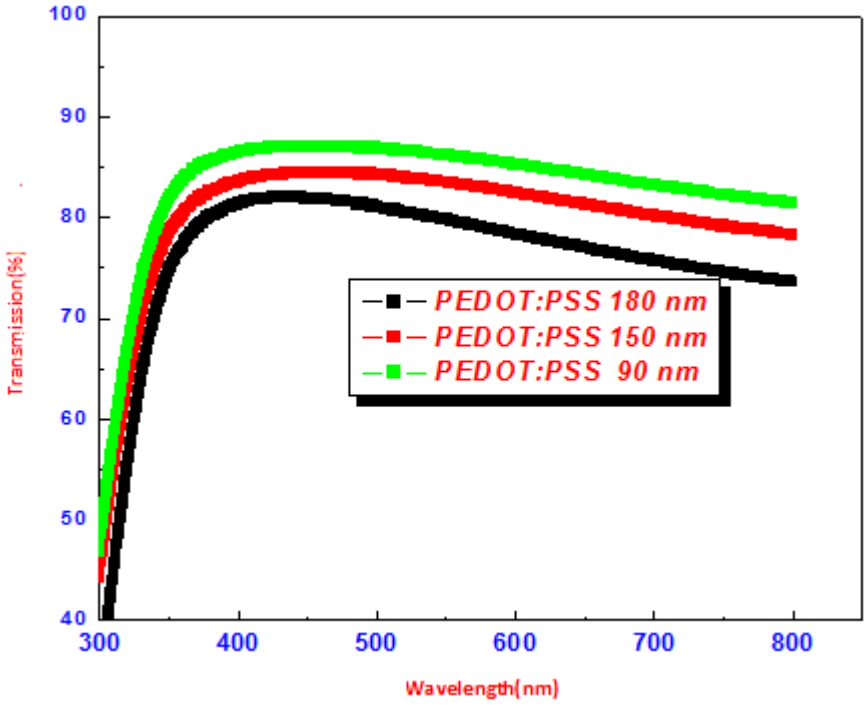

Figure 4.6: Transmission of PEDOT:PSS layer with different thickness

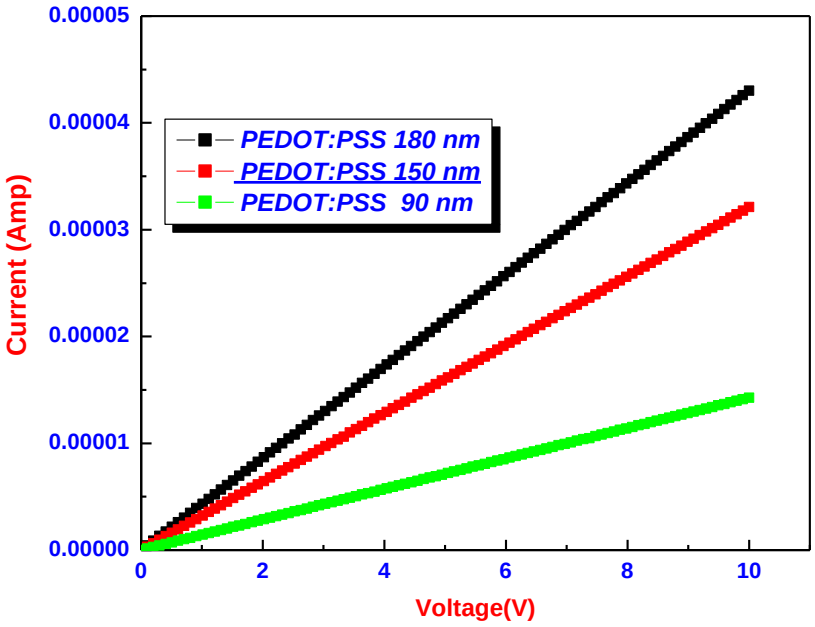

Figure 4.7: I-V curve of PEDOT:PSS layer with different thickness

Fig 4.8 shows the J-V characteristic of the solar cells with different thicknesses of PEDOT:PSS layers. We found that the V_{oc} of cells increases with increasing the thickness PEDOT:PSS layer but J_{sc} decreases slightly with increases thickness of PEDOT:PSS layer. The increment in V_{oc} is due to the change in work function with PEDOT:PSS layer thickness. As we have calculated that the work function increases as the thickness of PEDOT:PSS layer increases. But there is small decrement in current density with the increasing the thickness of PEDOT:PSS layer. As we see in Fig 4.8 the conductivity of PEDOT:PSS layer increases as the thickness of this layer increases, so the current density should be increased as the thickness of layer increases. But it is not the case here and indicates that the current density does not depend only the conductivity of material but also on the other phenomenon like photon absorption and charge collection in active layer. When the thickness of PEDOT:PSS layer increases the transparency of the device going to decrease due to this there is less absorption of photons in active layer. So there is slight decrement in current density with respect to increasing the PEDOT:PSS layer thickness.

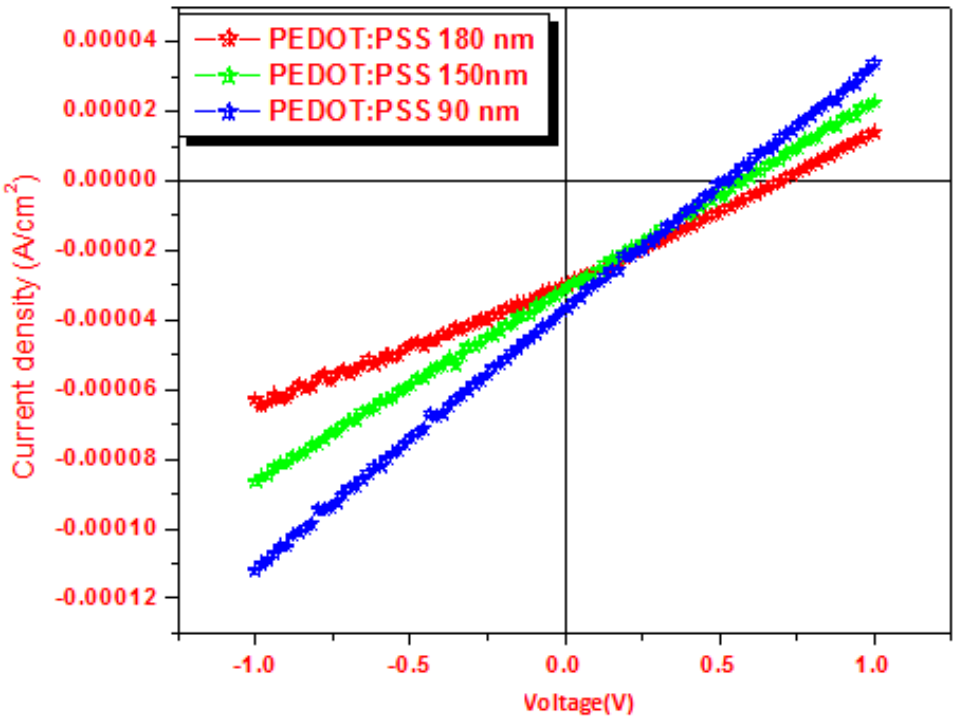

Figure 4.8: Cell performance with different thickness of PEDOT:PSS layer

4.4 Degradation study of P3HT:PCBM solar cell

4.4.1 Experimental details

Investigations have been carried out on the bulk-heterojunction solar cells based on the blend of P3HT and PCBM. P3HT was purchased from Aldrich Chemicals, USA, whereas PCBM was purchased from Nano-C, USA, and used as such. Samples were prepared on indium tin oxide (ITO) coated glass substrates (sheet resistivity ~ 18 Ω/□), which were patterned, cleaned and dried prior to device preparation. The cleaned substrates were exposed to oxygen plasma for 5 min. and a thin film of PEDOT:PSS (Aldrich Chemicals, 1.3 wt % dispersion in water) was spin coated on the ITO and cured at 120^{o}C for 20 min. in inert environment. The P3HT:PCBM solution (1:0.5, 25 mg/ml) in chlorobenzene was then spun over the PEDOT:PSS coated substrates and cured at 120^{o}C for 30 min. in the Glove box. Finally the samples were transferred to a thermal evaporator chamber, where Al electrodes (100 nm) were deposited under reduced pressure of ~ 1x10^{-6} mbar. The devices were taken

out of the evaporator chamber and tested in the ambient atmosphere (43±3 % rh, 27±3 ^{o}C) without encapsulation.

4.4.2 Result and discussion

After making the solar cell (ITO/PEDOT:PSS/P3HT:PCBM (1:0.5)/Al) the J-V characteristic are taken in open atmosphere. and recorded by the Keithley SourceMeter unit. A tungsten halogen lamp from Osram, Germany, was used to illuminate the cells at 100 mW/cm^2. For measurement of *J-V* characteristics the applied voltage was swept from -1V to +1V in the step of 0.02 V and the corresponding current was measured and recorded using Keithley 2420 SourceMeter unit interfaced with computer. Fig. 4.10(a) shows the dark and illuminated *J-V* characteristics of the non-encapsulated ITO/PEDOT:PSS/P3HT:PCBM (1:0.5)/Al solar cell measured just after preparation. The device exhibited J_{sc} of 3.41 mA/cm^2, V_{oc} of 0.60 V, FF of 49.6 % and η of 1.01 %. .In initial stage the performance the cell showed the fast degradation with respect to time and after that cell degrades slowly. Fig 5.1 cell performance in initial condition.

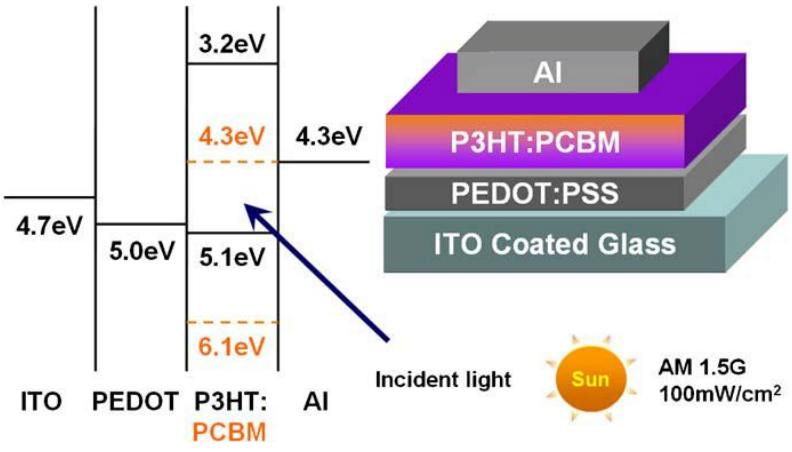

Figure 4.9: The energy diagram for ITO/PEDOT:PSS/P3HT:PCBM/Al cell.

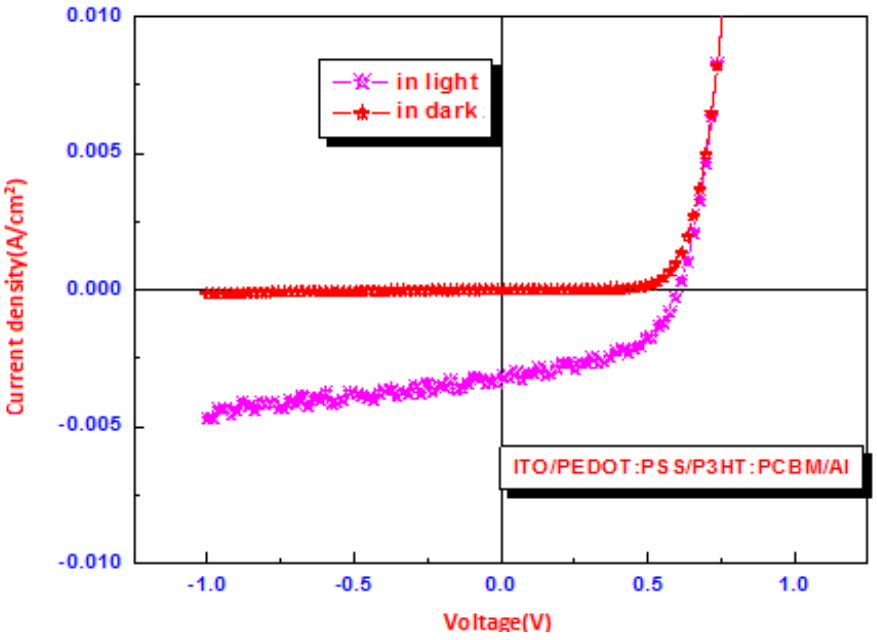

Figure 4.10 (a): Initial performance of ITO/PEDOT:PSS/P3HT:PCBM/Al solar cell.

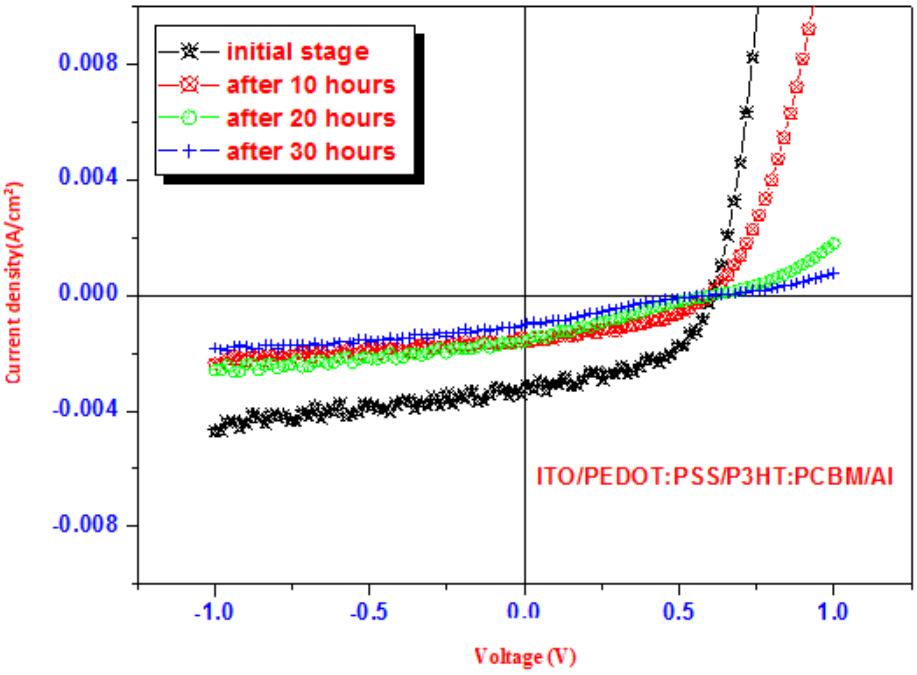

Figure 4.10(b): Degradation of ITO/PEDOT:PSS/P3HT:PCBM/Al cell with time

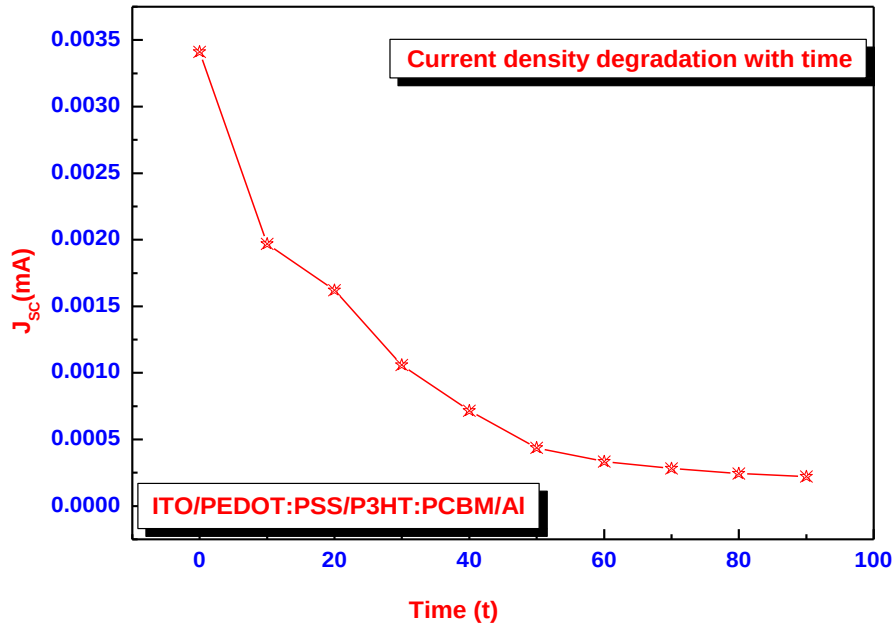

Figure 4.10 (c): Degradation in current density with respect to time

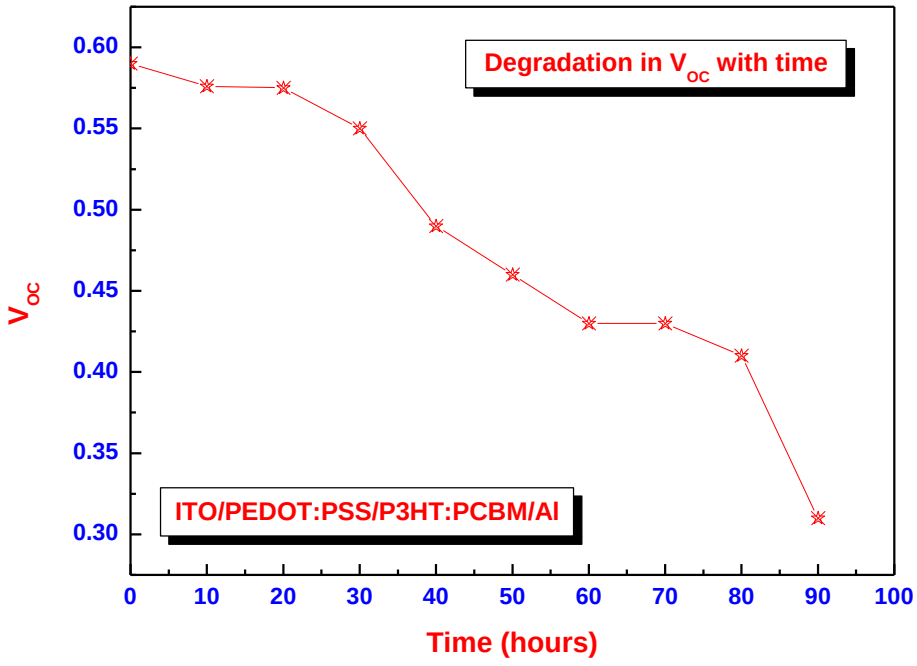

Figure 4.10(d): Degradation in V_{oc} with time

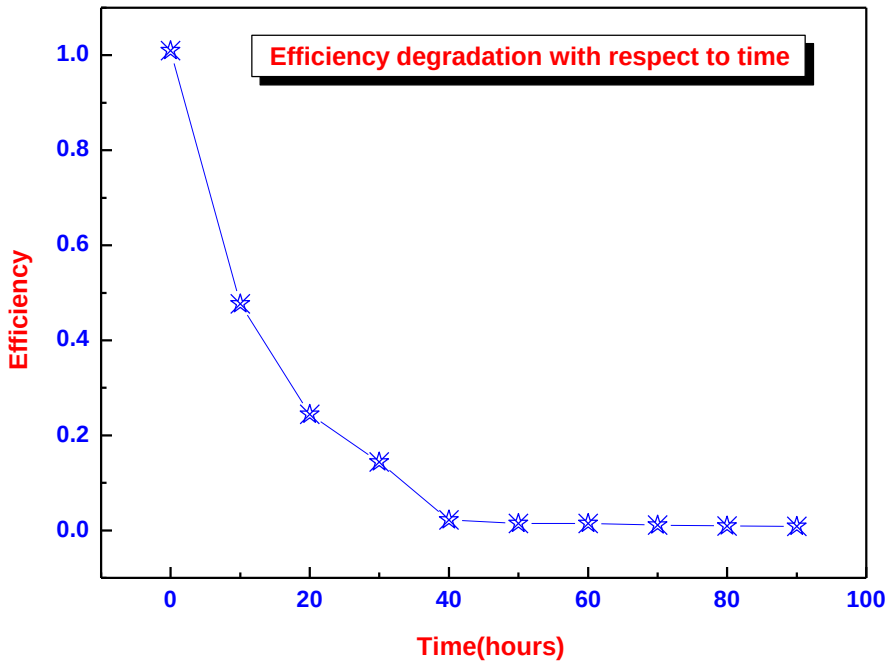

Figure 4.10 (e): Degradation in efficiency with respect to time

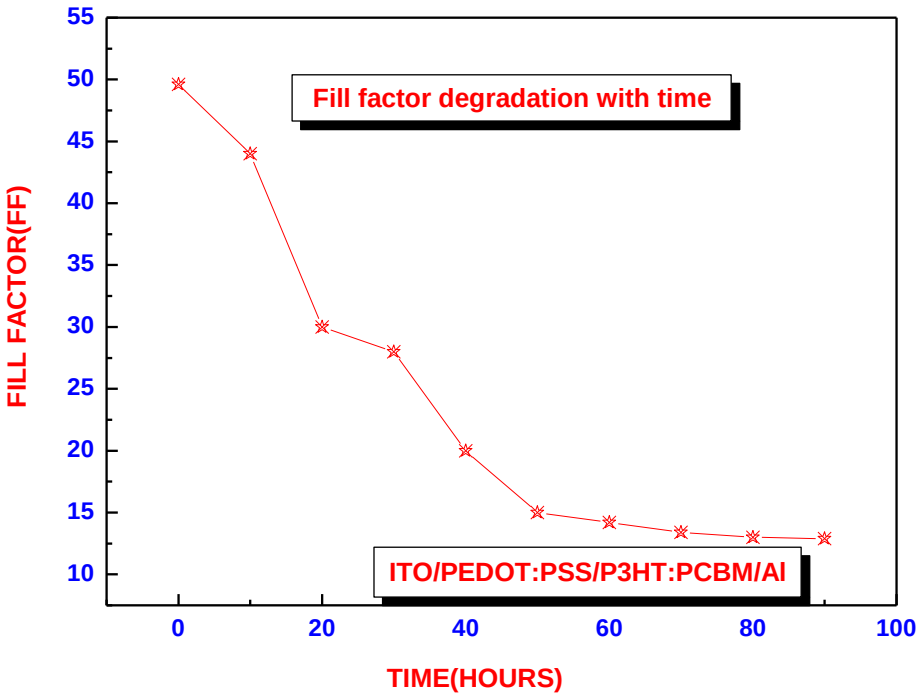

Figure 4.10 (f): Degradation in current Fill factor(FF) with respect to time

These figures 4.10 (a), (b), (c) ,(d) ,(e) ,(f) shows that the current density, efficiency, and fill factor decreases fastly in initial stage and then decreases slowly but open circuit voltage (V_{oc}) decreases slowly as compare to Jsc , FF, and efficiency. Open circuit voltage (V_{oc}) exhibited almost linear decay with time.

We did calculate the series (R_s) and shunt (R_{sh}) resistances of the device both in dark and under illumination. Fig.4.11 shows the variation of R_s and R_{sh} of the device with time calculated in dark. R_s and R_{sh} were extracted from the slop of the *J-V* characteristics in first and third quadrants near the points corresponding to V_{oc} and J_{sc} respectively. Initially both the R_s and R_{sh} were observed to increase very fast and afterwards slowly with time. The device showed very slight variation in R_s in dark and under illumination whereas R_{sh} exhibited large variation in dark and under illumination. Compared to the values in dark R_{sh} exhibited lower values under illumination.

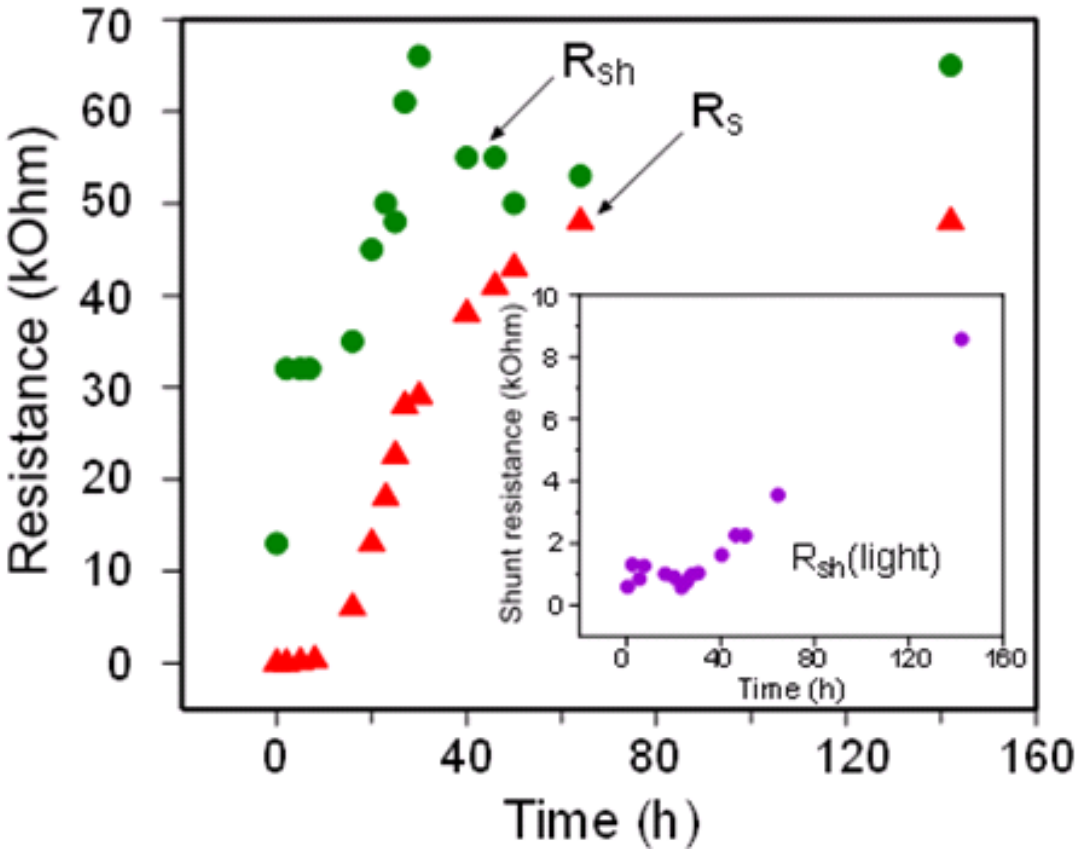

Figure 4.11: Change in series (R_s) and shunt (R_{sh}) resistances of the device both in dark and under illumination with time.

Inset of Fig 4.11 shows the variation of R_{sh} with time under illumination. The reduction of R_{sh} under illumination can be attributed to the photo-induced doping and is done by adding a photo conductive parallel resistance, where photoconductivity is proportional to the light intensity **[47]**. Initially (at t = 0 h) the device exhibited R_s = ~ 5.2 Ω which increased to ~ 4.8×10^4 Ω just after ~ 60 h. Similarly the R_{sh} which initially (at t = 0 h) was 1.3×10^4 Ω, increased to ~ 5.3×10^4 Ω after ~ 60 h in dark. Similarly the initial value of R_{sh} in light 5.61×10^2 Ω increased to 3.5×10^3 Ω, after ~ 60 h. These variations became more pronounced with time.

The increment in R_s could originate from several factors viz. increase in the resistivity of PEDOT:PSS, increase in the charge injection barrier to active layer and reduction in charge carrier mobility in the active layer. On the other hand increment in R_{sh} with time can be attributed to the change in the nano-scale morphology, phase separation and formation of dead zones in the active layer, which minimizes the shorts and reduces the leakage current. Therefore reduction in J_{sc} on degradation can now be attributed to increase in the series resistance, reduction in the internal electric field due to electrode degradation, oxygen induced doping of P3HT:PCBM and increment in the trapping density, which reduces the charge carrier mobility **[48]**. V_{oc} in organic solar cells is controlled by both the difference of work function of the electrodes used and difference of highest occupied molecular orbital (HOMO) of donor and lowest unoccupied molecular orbital (LUMO) of the acceptor molecules **[49]**. The change in V_{oc} in the present case can be attributed to the change in the work function of the ITO/PEDOT:PSS electrode. Due to hygroscopic nature of PEDOT:PSS it absorbs water and losses its electronic properties, and as a result the work function reduces. Along with that because of acidic nature of PEDOT:PSS, it etches ITO and changes its properties.

Studies show that from ITO, In diffuses into active layer and even to Al electrode **[50]**. Such changes do modify the work function of ITO. Because of creation of more free electrons in ITO, the Fermi level goes up. Now the difference between work functions of ITO/PEDOT:PSS and Al reduces, which results into the reduction in V_{oc}. Also the imbalance charge carrier mobilities due to degradation will result formation of space charge and as a result reduction in V_{oc}. After some time (~ 142 h for present device) this difference diminishes and device exhibit no photovoltaic response. The device exhibited complete degradation in ~ 142 h with all parameters showing fast degradation and after 142 h the performance became zero i.e. both the dark and illuminated characteristics pass through the

origin. When the device is completely degraded though it is not short circuited but J_{sc} disappears because of the absence of built in electric field **[51]**.

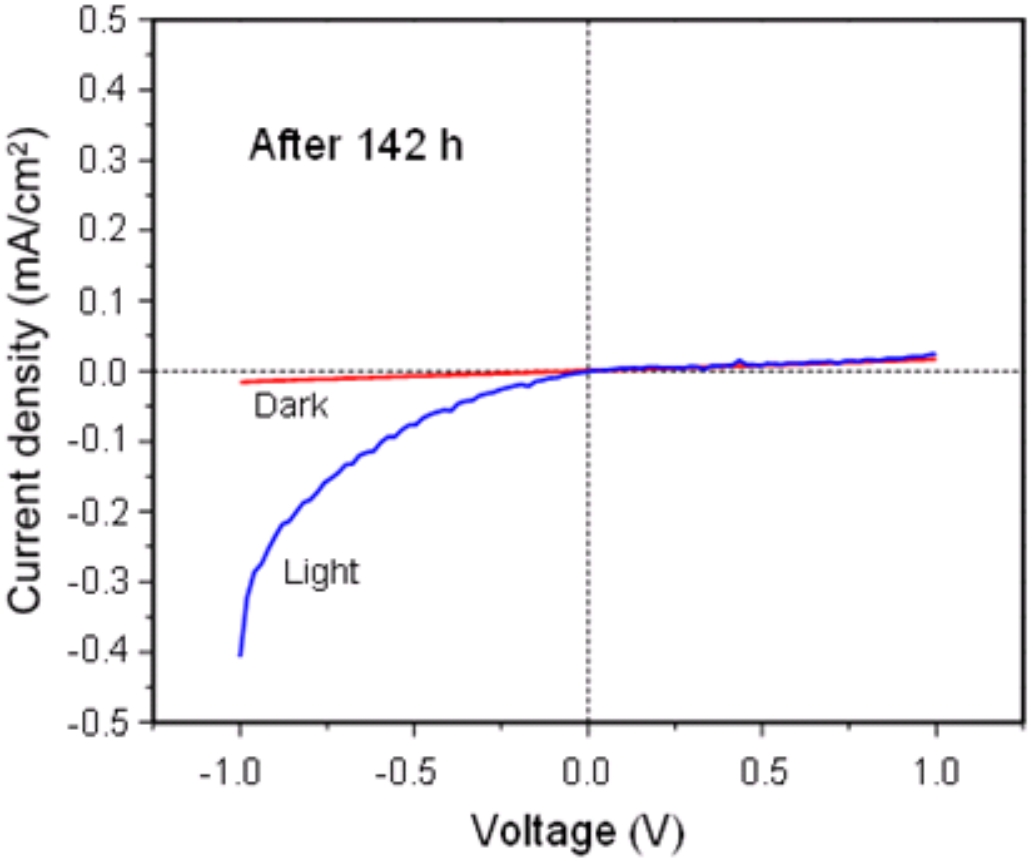

Figure 4.12: Complete degradation of device in dark and light after 142 hours.

After complete degradation when the device was dead we did further measure the *J-V* characteristics with time and found very interesting result that both the dark and illuminated characteristics started passing through the second quadrant. Regular measurement of the characteristics revealed that both the characteristics kept regularly shifting into the second quadrant with time. To reconfirm this observation a new device was prepared in the same configuration and in the similar procedure. Initially the device exhibited J_{sc} = 4.63 mA/cm^2, V_{oc} = 0.56 V, *FF* = 46.8 %, and η = 1.2 %. This device also exhibited the same degradation behavior as that of the device discussed above. Interestingly when this device as well was completely dead after ~ 200 h, further measurement of *J-V* characteristics with time showed the same behavior and characteristics started passing through the second quadrant. This is quite interesting result as we get the current at zero voltage in the dark.

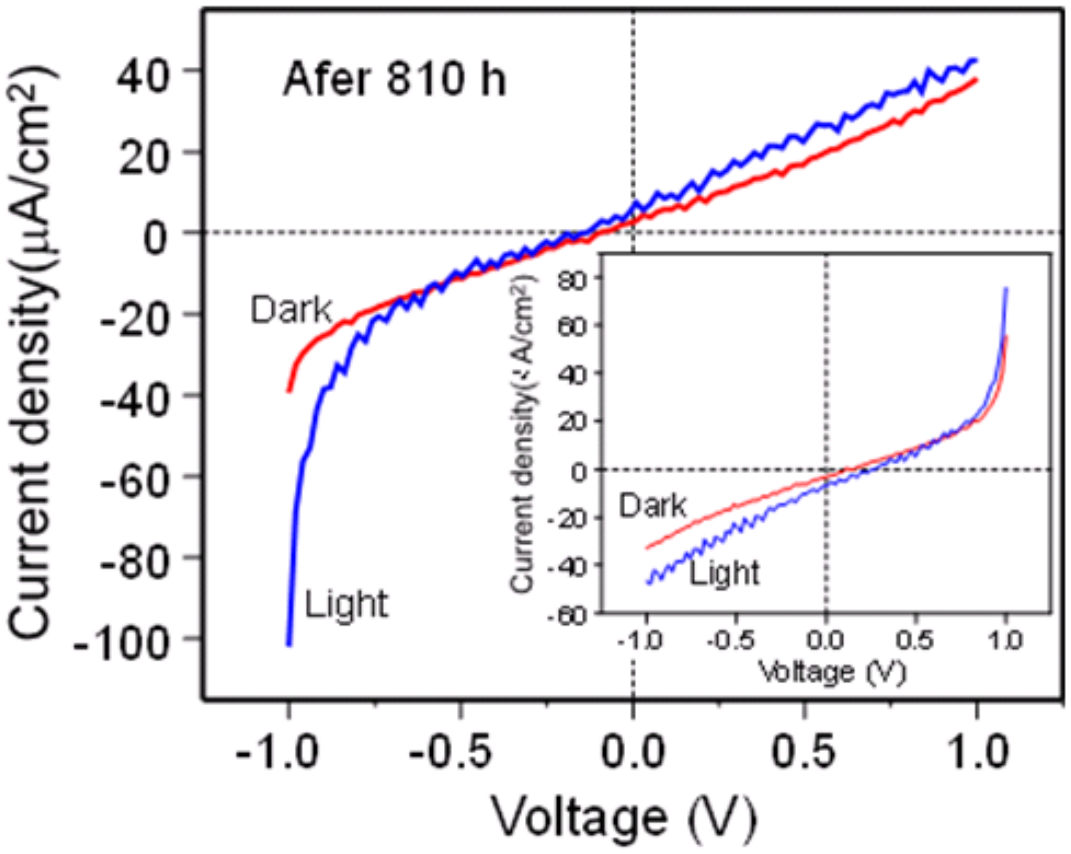

Figure 4.13: J-V characteristics of the second device after 810 h

Fig. 4.13 Shows the *J-V* characteristics of the second device after ~ 810 h. To find out the reason behind this shifting we did carry out the detailed investigations. As mentioned above for the measurement of *J-V* characteristics, normally the voltage was swept from -1 V to +1 V (forward sweep) in the step of 0.02 V, but for detailed understanding we also measured the characteristics by sweeping the voltage from +1 V to -1 V (reverse sweep). Interestingly this time the characteristics passed through the fourth quadrant in both the dark and under illumination. Inset of Fig 4.13 shows the dark and illuminated characteristics of the device after ~ 810 h when the voltage was reverse swept from +1 V to – 1 V. In dark the characteristics intersected the V-axis at – 0.10 V and 0.15 V for forward and reverse sweep respectively. In case of light illumination the voltages at which characteristics intersect V-axis was slightly more than that in the dark and was observed to be – 0.13 V and 0.25 V for forward and reverse sweeps respectively. The possible mechanism that could account for these observations is the polarization of P3HT molecules, which happen due to its degradation .

This may happen along with the change in the effective work function of PEDOT:PSS via change in carrier density near the active layer-PEDOT:PSS interface or formation of dipole layer at the interface. It is worth mentioning that we did measure the characteristics of the freshly prepared devices as well by sweeping the voltage from –ve to +ve and +ve to –ve and interestingly found absolutely no difference in the characteristics rather an excellent overlap. Dark characteristic was observed to pass through the origin (0,0) and the illuminated characteristic passed through fourth quadrant. No difference in the characteristics (in the common voltage range) was observed even when the characteristics were measured for different voltage sweep.

It is known however, that P3HT form a charge transfer complexes with oxygen, resulting formation of cation and anion radical species, which can be detected by electron spin resonance (ESR). Formation of these charged ions represents the doping of P3HT. This doping increases with degradation of P3HT and increment in oxygen concentration. It was found that a sample under vacuum contained ~ 5.4×10^{17} spins g^{-1} (electrons). In oxygen (1 atm), the spin density increased more than ten-fold to ~ 7.1×10^{18} spins g^{-1} **[52]**. As a consequence the conductivity of P3HT increases with oxygen concentration. It is known that thiophenes undergo degradation at room temperature as shown in the scheme below **[53]**.

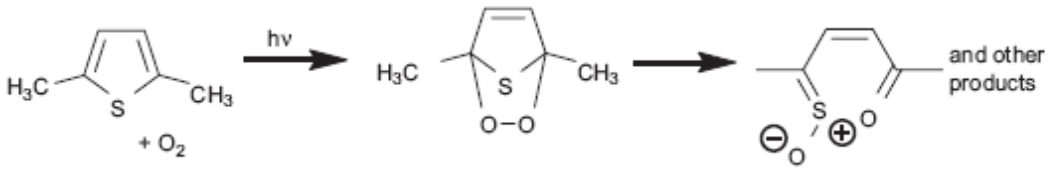

The formation of charge transfer complexes between oxygen and P3HT was investigated via oxygen-induced fluorescence quenching by Luer *et al.* **[54]**. The authors suggest that the reaction involves metastable oxygen species that are later responsible for the irreversible degradation of the polymer. This formation of charge transfer complex results into the *p*-type doping of P3HT **[55, 56]**. The electron transfer from P3HT to oxygen molecule results into the formation of mobile holes on P3HT and immobile electrons on oxygen. The oxygen induced degradation of P3HT decreases the charge carrier mobility and increases the trap densities **[48]**. Whereas in case of fullerenes the oxygen doping reduces

electron concentration **[57,58]**. Norrman *et al.* did investigate the oxygen uptake in P3HT:PCBM solar cell and the intensities of the fragment ions was studied by TOF-SIMS spectroscopy **[59]**. It has been found that in P3HT sulphur reacts with water and/or oxygen in ambient which increases $C_xH_ySO_z^-$ and SO_x^- concentration. The reduction in $C_xH_yS^-$ ions and increment $C_xH_yO_z^-$ ions suggest that either the thiophene carbon in P3HT becomes oxygenated or the side chains are oxygenated. The TOF-SIMS images of the PEDOT:PSS surfaces reveal that the layers have phase separated into a PEDOT-rich and a PSS-rich phase. Each phase was identified from area-specific TOF-SIMS mass spectra.

Therefore when the device is completely degraded the active layer exhibits charged ions and when an external voltage is applied they get polarized in the opposite direction to the applied electric field. In case of characteristics measured in forward sweep from -1 V to + 1 V, the anions get attracted towards positively biased electrode and cations towards negatively biased electrode and the active layer gets polarized.

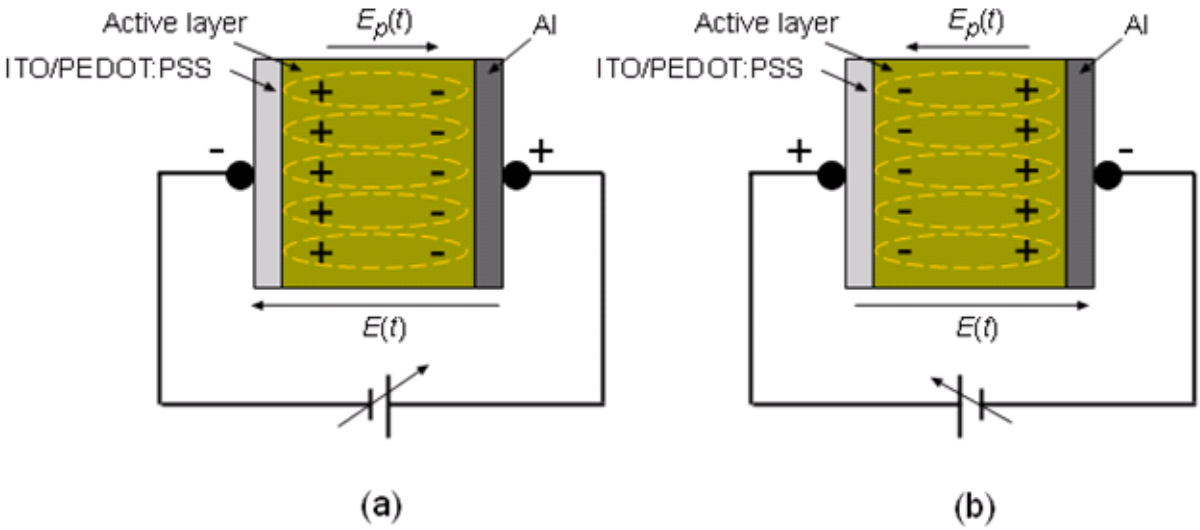

Fig 4.14. Schematic representation of polarization of the active layer on the application of forward and reverse bias.

Polarization of the active layer develops an internal electric field which opposes the applied external electric field (see Fig. 4.14 (a)). $E(t)$ represents the applied electric field whereas $E_p(t)$ corresponds to the induced electric field due to polarization. The developed internal electric filed pushes the charge carriers in the opposite direction to that due to applied

electric field. At -1 V current is dominantly controlled by applied voltage and remains –ve in magnitude.

As the applied voltage decreases towards 0 V and when it becomes equal to the induced voltage (due to polarization) the effective internal voltage become zero and as a result total current becomes zero. This is the point where characteristic intersects the V-axis in –ve direction. As the applied voltage decreases further the effect of polarization induced voltage become dominant and the direction of current changes. This is because we get a +ve current at the zero applied voltage and when the applied voltage get reversed to +ve direction current increases as the voltage increases further because the current due to applied voltage and due to polarization are now in the same direction. In case of reverse sweep from +1 V to -1 V the active layer this time gets polarized in the opposite direction and again the polarization induced voltage opposes the applied voltage (see Fig. 4.14 (b)). When the applied voltage and polarization induced voltage become equal the current again becomes zero and this is the point where characteristic intersects the V-axis in +ve direction. Now when the applied voltage reduces the current due to induced voltage start dominating and current becomes –ve. This is why in this case we get a –ve current at zero voltage. When the applied voltage get reversed to –ve direction and increases in magnitude the current due to applied voltage adds up into the current due to polarization as they are now in the same direction. The total current increases with increment in the applied voltage.

To establish this concept we did perform detailed experiments where investigations were also carried out for higher applied voltage range viz. + 2 V to – 2 V and – 2 V to + 2 V. Fig.4.15shows the dark and illuminated characteristics after ~ 1250 h, when the voltage was swept from -1 V to +1 V and +1 V to – 1 V. In dark the characteristics intersected the V-axis at – 0.13 V and 0.17 V for forward and reverse sweep respectively. In case of light illumination the voltages at which characteristics intersect V-axis was slightly more than that in the dark and was observed to be – 0.23 V and 0.29 V for forward and reverse sweep respectively.

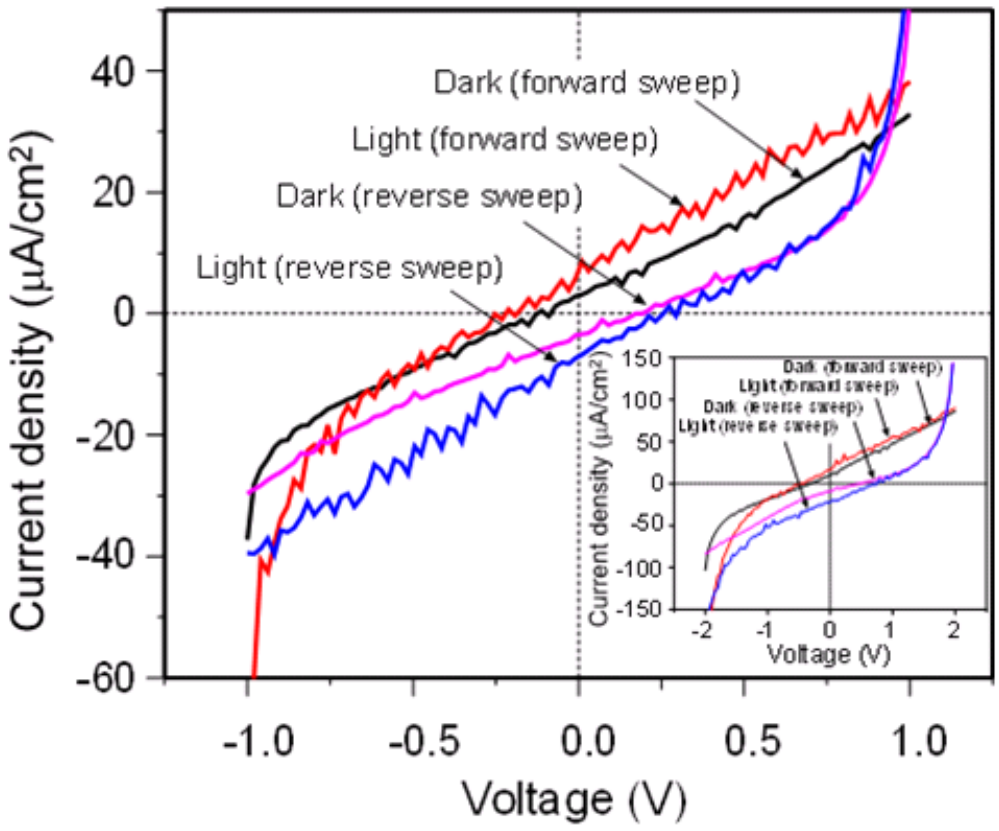

Fig 4.15: *J-V* characteristics of the degraded solar cell after ~ 1250 h, measured in dark and under illumination in both the forward and reverse voltage sweeps in the voltage range ± 1 V.

The inset shows the dark and illuminated characteristics measured at the same time for the voltage sweeps from -2 V to +2 V and +2 V to – 2 V. Interestingly the voltages at which characteristics intersect the V-axis increased to -0.34 V and 0.5 V in dark and -0.5 V and 0.78 V in light for forward and reverse sweeps respectively. These higher voltages of intersection for voltage sweep of ± 2 V compared to that for ± 1 V at the same time is quite interesting. The experiments were also carried out for other higher voltage ranges as well and the results were found in consistency with observed for lower voltages discussed above. We measured the characteristics again and again to confirm the reproducibility of the behaviour and found absolutely no difference and excellent reproducibility. These results can again be explained by the concept of polarization of active layer. Since in case of voltage sweep from -2 V to +2 V and +2 V to – 2 V, the applied voltage is more therefore the polarization will be more and as a result the induced voltage will be more. Because of more induced voltage due to polarization, the voltage, where current become zero while sweeping from – 2 V to + 2 V,

will be more than that for the case of voltage sweep from – 1 V to + 1 V, and because of that the current at zero applied voltage will be more due to more polarization in the case of the voltage sweep from -2 V to + 2 V. Similarly the characteristics for the voltage sweep from +2 V to -2 V can be explained. In this case as well the voltage where characteristic intersects the V-axis will be more than that in case of voltage sweep from +1 V to -1 V.

Under illumination the voltages where characteristic intersects the V-axis and the currents at zero voltage both are more in both the reverse and forward sweeps compared to that in dark. This observation is true for all the voltage ranges and can be explained as follows. Under illumination more charge carriers are generated and contribute to the polarization or in other term the polarization induced voltage. Since the photo-generated charge carriers contribute to polarization the voltage where characteristics will intersect the V-axis and the current at zero applied voltage will be more than that in the dark.

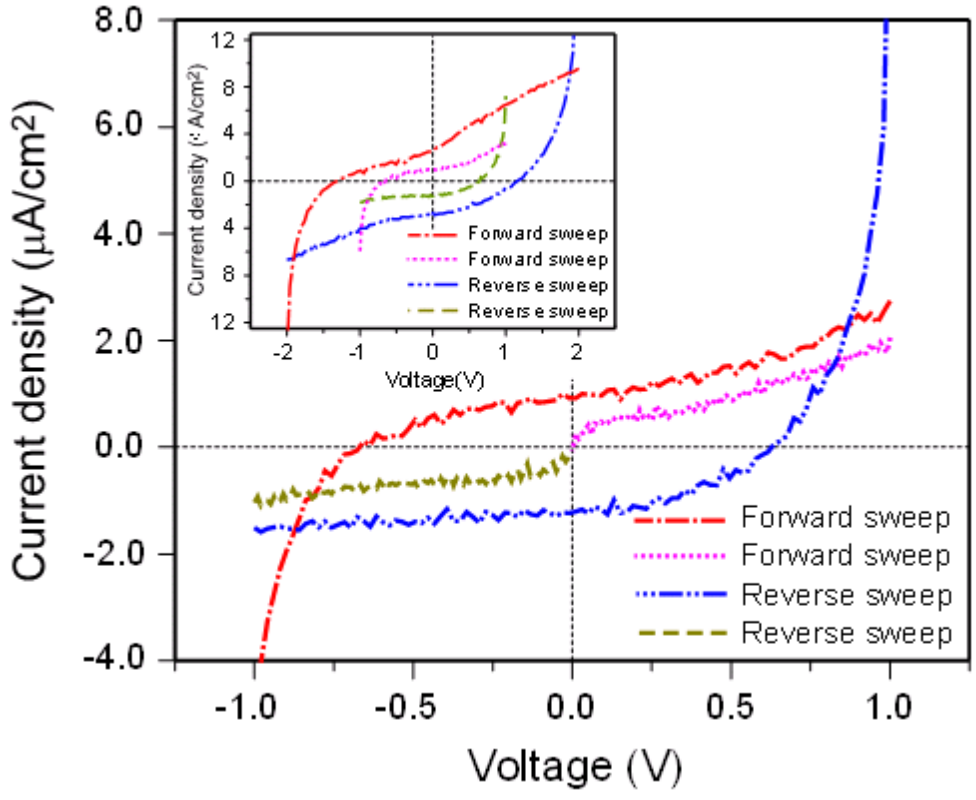

Figure 4.16: *J-V* characteristics of a seriously degraded solar cell measured in dark and under illumination for forward and reverse voltage sweeps. Dotted curve is for the measurement from 0 V to +1 V whereas dashed curve is for the measurement from 0 V to – 1 V. Inset shows the dark and illuminated *J-V* characteristics for two voltage ranges ± 1 V and ± 2 V, measured at the same time in forward and reverse sweeps.

We did also performed the experiments where voltage was swept from 0 to + ve voltage and 0 to –ve voltage as well and interestingly found different characteristics compared to those measured while sweeping from –ve to +ve and +ve to –ve voltage respectively. When the voltage was swept from 0 V to either -2 V or +2 V the characteristics passed through origin in both the dark and under illumination, which suggest no photo current at zero applied voltage

This can be understood from physical consideration that when the applied voltage is swept from 0 V no polarization will take place because the applied voltage is zero, though the polarization will take place as the applied voltage increases. The current at any voltage is different for the cases when voltage is swept from –ve to +ve or +ve to –ve voltage and 0 to +ve voltage or 0 to –ve voltage, because the magnitude of polarization will be different in the different cased. Since there is no photocurrent at zero applied voltage, the current at higher voltages under illumination was more than that in dark, which suggests photo-generation of charge carriers at high voltages. This photo-generation of charge carriers is because of exciton dissociation due to applied voltage.

Chapter 5
Conclusions ,Summary and Future plan

5.0 Conclusions

So after seeing the degradation of devices we concluded that device ITO/PEDOT:PSS/P3HT:PCBM/Al shows the fast degradation in comparison to the devices ITO/P3HT:PCBM/Al because of poor stability of the interface between ITO and PEDOT:PSS. In case ITO free solar cells (PEDOT:PSS/P3HT:PCBM/Al) the current density was very small due to the low mobility of PEDOT:PSS but open circuit voltage (V_{oc}) was high as compared to devices with ITO. Degradation study of these devices showed that current density of these devices decreases very fastly due to increment in resistivity of PEDOT:PSS layer in open atmosphere. But there was very small decrement in Voc with respect to time. So if we avoid the ITO electrode. However, due to the higher series resistances, the low values of photocurrent make realisation of this cells using only PEDOT:PSS as transparent conducting electrode (without ITO), not interesting for instance, but this indicates that more conductive films of PEDOT:PSS could lead to a free ITO solar cells and consequently to lower cost and longer lifetime full organic solar cells.

In conclusion we have performed the degradation studies in P3HT:PCBM solar cells. Studies show exponential decay in J_{sc} and η, whereas V_{oc} has been observed to decay linearly. Reduction in Jsc has been attributed to increment in series resistance, reduction in charge carrier mobility and introduction of traps whereas reduction in V_{oc} has been attributed to reduction in the difference of workfunction of the electrodes. Detailed investigations show that degradation results into formation of charged ions in the active layer which get polarized when an external voltage is applied to the device. This polarization increases with degradation of active layer and applied voltage. The polarization of the active layer exhibits interesting effect on the device characteristics and charge carrier transport.

5.1 Summary

The objective of this thesis work was to fabricate polymer solar cells and investigate the degradation with time. For this purpose P3HT and PCBM were respectively selected as the donor and acceptor materials and the devices were prepared in bulk-heterojunction configuration, where P3HT and PCBM were blended together to form a single active layer. Devices were fabricated in sandwich structure on glass substrates where active layer was sandwiched between transparent anode (ITO and/or ITO/PEDOT:PSS) and opaque cathode (Aluminum). A typical structure of the studied solar cells was ITO/PEDOT:PSS/P3HT:PCBM/Al. Prior to degradation studies we optimized the blend ratio for P3HT and PCBM and then studied the degradation on the optimized device. The devices were prepared in 1:0.5, 1:0.8, 1:1 and 1:1.5 ratios of donor and acceptor materials. For these studies P3HT and PCBM were from Aldrich Chemicals USA and were used as received. We studied the photovoltaic performance and found that 1:1 ratio is the optimum ratio for efficient photo-conversion. The variation in the performance with change in the ratio of the donor-acceptor materials can be attributed to the change in the nano-scale morphology and electronic properties of the active layer. After device optimization the devices were subjected to the degradation studies where we studied the performance of the devices time to time.

We have also investigated the effect of PEDOT:PSS on degradation of P3HT:PCBM solar cells. For this purposes devices were prepared for different thicknesses of PEDOT:PSS and even without PEDOT:PSS. PEDOT:PSS has been found to be the main source of degradation of these devices. The device incorporating PEDOT:PSS exhibited poorer stability compared to that without PEDOT:PSS. The poor stability of the devices incorporating PEDOT:PSS can be attributed to the degradation of PEDOT:PSS, which etches ITO, resulting diffusion of In into active layer. PEDOT:PSS is hygroscopic in nature and absorbs water. The acidic nature of PEDOT:PSS etches ITO. It is seen that PEDOT:PSS loses its conductivity with time resulting increase in series resistance and reduction in Jsc. We studied the performance of the solar cells with time and found that both the Jsc and Voc degrade exponentially with time, whereas Voc decreases almost linearly. We did calculate the series (R_s) and shunt (R_{sh}) resistances of the device both in dark and under illumination. Initially both the R_s and R_{sh} were observed to increase very fast and afterwards slowly with time.

When the devices were completely dead (all the parameters Jsc, Voc, FF and efficiency became zero), we further studied the *J-V* characteristics with time and observed some interesting features. For the measurement of *J-V* characteristics the voltage was swept from -1 V to + 1V (forward sweep) in the step of 0.02 V. The measurement of *J-V* characteristics with time on the completely degraded device showed that the characteristics started passing through the second quadrant. This is quite interesting result as we get the current at zero voltage in the dark. For detailed understanding we also measured the characteristics by sweeping the voltage from +1 V to -1 V (reverse sweep). Interestingly this time the characteristics passed through the fourth quadrant in both the dark and under illumination. These results have been analyzed and studied in detail and the possible mechanism that could account for these observations is the polarization of P3HT molecules, which happen due to its degradation. This may also happen along with the change in the effective work function of PEDOT:PSS via change in carrier density near the active layer-PEDOT:PSS interface or formation of dipole layer at the interface. These results are very important to understand the degradation mechanism in polymer solar cells.

5.2 Future plan

Polymer solar cells are considered to be the future source of energy as they promise for thin, flexible, large area solar cells at very low cost. This is a quite environmental friendly technology and produce energy direct from sun light. Efficiency and life time of these devices are not sufficient enough for their commercialization. If the technology has to come out of the laboratories and reach the market more detailed research and development work is urgently required. Research is being done all over the world in this direction. My future plan is to work in the same area and specifically the understanding of degradation mechanism and long term stability of these devices. I wish to work in more detail on prevention of polymer solar cells from degradation so that we could realize long term stable solar cells, helping in realization of their commercialization.

REFERENCES

[1] http://en.wikipedia.org/wiki/Renewable energy.

[2] N. Norbrook, G. Mithembu-Salter, Africa Report, 2007.

[3] D. Y. Goswami, Advances in Solar Energy: An Annual Review of Research and Development, 7 (2003).

[4] C. Brabec, U. Scherf, V. Dyakonov, Eds., And Organic Photovoltaics: Materials, Device Physic s, and Manufacturing Technologies; Wiley-Vch, 2008.

[5] V. Petrova-Koch, R. Hazel, A. Goetzberger, Eds., High-Efficient Low-Cost Photovoltaics; Springer Series in Optical Sciences, 2009.

[6] S.-S. Sun, N. S. Sariciftci, Eds., Organic Photovoltaic's: Mechanisms, Materials, and Devices; Marcel Dekker Inc, 2005.

[7] A. Smee, Elements of Electro-Biology London: Longman, Brown, Green, and Longmans, 1849.

[8] Halls, J. J. M., Cornil, J., dos Santos, D. A., Silbey, R., Hwang, D. H., Holmes, A. B., Brédas, J. L. & Friend, R. H. 1999. Charge- and energy-transfer processes at Polymer/polymer interfaces: A joint experimental and theoretical study. Physical Review B, 60, pp.5721-5727.

[9] Energy Information Administration. 2006. International Energy Outlook 2006. report DOE/EIA-0484.

[10] D. M. Chapin, C. S. Fuller, G. L. Pearson, A new silicon p-n junction photocell for converting solar radiation into electrical power, J. Appl.Phys. 25, 676 (1954).

[11] Solar Cell Efficiency Tables (Version12), Progress in Photovoltaics: Research and Applications 7 (1998).

[12] W. Shockley and H. J. Queisser, Detailed balance limit of efficiency of PN junction solar cells, J. Appl.Phys. 32, 510 (1961).

[13] A. Goetzberger, C. Hebling, H. W. Schock, Photovoltaic materials, history, status and outlook, Materials Science & Engineering R-Reports 40, 1 (2003).

[14] International Energy Agency. 2007. Renewables in Global Energy Supply - An IEA Fact *Sheet.*

[15] Genes, S., Neugebauer, H. & Sariciftci, S. N. 2007. Conjugated Polymer-Based Organic Solar Cells. Chemical Reviews, 107, pp.1324-1338.

[16] Liang Y, Xu Z, Xia J, Tsai ST, Wu Y, Li G, Ray C and Yu L, Adv. Mater, **22** E135 (2010).

[17] Stephen R. Forrest, MRS bulletin 30, 28-32 (2005).

[18] M. Knupfer, Appl. Phys. A: Mater. Sci. & Proc., 77, 623-626 (2003).

[19] C. K. Chiang, C. R. Fincher, Y. W. Park, A. J. Heeger, H. Shirakawa, E. J. Louis, S. C. Gau, and A. G. MacDiarmid: Electrical conductivity in doped polyacetylene. Phys. Rev. Lett., Vol. 39, 1098 (1977).

[20] R. N. Marks et al., J. Phys.: Condens. Matter 6, 1379 (1994).

[21] M. Knupfer, Appl. Phys. A: Mater. Sci. & Proc. 77, 623-626 (2003).

[22] C. W. Tang, Appl. Phys. Lett. 48, 183 (1986).

[23] J. M. Halls et al., Appl. Phys. Lett. 68, 3120 (1996).

[24] L. S. Roman L.A.A. Patterson, and O. J. Inganas J.Appl. Phys. 86, 487 (1999).

[25] M. Theander et al., O. Phys. Rev. 61, 12957 (2000).

[26] Aharon Yakimov Peter Peumans and Stephen R. Forrest, J. Appl. Phys. 93, 3693(2003).

[27] N.D. Sacriciftci, Appl. Phys. Lett. 62, 585 (1993).

[28] G. Yu and A. J. Heeger, J. Appl. Phys. 78, 4510 (1995).

[29] Gang Li et al., Nature Materials 4, 864 (2005).

[30] Y. Kim et al., Nature Materials 5, 197 (2006).

[31] P. W. M. Blom, V. D. Mihailetchi, L. J. A. Koster, D. E. Markov, Adv. Mater. 2007.

[32] http://en.wikipedia.org/wiki/Exciton.

[33] A. Haugeneder, M. Neges, C. Kallinger, W. Spirkl, U. Lemmer, J. Feldmann, U. Scherf, E. Harth, A. Gügel, K. Müllen, Phys. Rev. B, 59, 15346 (1999).

[34] L. A. A. Pettersson, L. S. Roman, O. Inganäs, J. Appl. Phys. 86, 487 (1999).

[35] R. H. Bube, Photoelectronic Properties of Semiconductors, Cambridge University Press, Cambridge, 1992.

[36] M. Pope, C. E. Swenberg, Electronic Process in Organic Crystals and Polymers, Oxford University Press, Oxford, 1999.

[37] S.-S. Sun, N. S. Sariciftci, Organic Photovoltaics Mechanisms, Materials, and Devices, CRC Press, 2005.

[38] C. Brabec, U. Scherf, and V. Dyakonov, Organic Photovoltaics, Wiley VCH, Weinheim, Germany, 2008; (b) C. Deibel, Phys. Status Solidi A, 12, 2731(2009).

[39] http://www.physik.uni-wuerzburg.de/EP6/research-oe.html.

[40] H. B. Michaelson, "The work function of the elements and its periodicity," Journal of

Applied Physics, vol. 48, no. 11, pp. 4729–4733, (1977).

[41] J. M. Bharathan and Y. Yang, "Polymer/metal interfaces and the performance of polymer light-emitting diodes," Journal of Applied Physics, vol. 84, no. 6, pp. 3207–n 3211, (1998).

[42] Y. Park, V. Choong, E. Ettedgui, et al., "Energy level bendingvand alignment at the interface between Ca and a phenylenevvinylene oligomer," Applied Physics Letters, vol. 69, no. 8, pp. 1080–1082, (1996).

[43] Kim, S.C., Naidu, B.V.K., Shim, J.M., Jung, S.J., Shin, W.S., Jin, S.H., Lee, J.K., Lee, J.W., and Gal, Y.S., Polymeric photovoltaic devices based on tricomponent system Composed of a blend of donor and PCBM acceptor material. Molecular Crystals and Liquid Crystals, 471: p. 137-145(2007).

[44] Jørgensen, M., Bundgaard, E., Bettignies, R.d., and Krebs, F.C., Chapter 2: The Polymer Solar Cell, in Polymer Photovoltaics, A Practical Approach Editor: F.C. Krebs.

[45] Li, C.Y., Wen, T.C., Lee, T.H., Guo, T.F., Huang, J.C.A., Lin, Y.C., and Hsu, Y.J., An inverted polymer photovoltaic cell with increased air stability obtained by employing novel hole/electron collecting layers. Journal of Materials Chemistry, 19(11): p. 1643-1647(2009).

[46] R. Schlaf, H. Murata, Z.H. Kafafi, Work function measurements on indium tin oxide Films, J. Electron Spectrosc. Relat. Phenom. 120 ,149–154(2001).

[47] P. Kumar, S. C. Jain, V. Kumar, S. Chand, R. P. Tandon, J. Appl. Phys. 105, 104507 (2009).

[48] J. Schafferhans, A. Baumann, A. Wagenpfahl, C. Deibel, and V. Dyakonov, Org. Electron. 11, 1693 (2010).

[49] P. Kumar, S. Chand, Prog. Photovolt. Res. Appl. (2011) (in press).

[50] D. E. Gallardo, C. Bertoni, S. Dunn, N. Gaponik, A. Eychmüller, Adv. Mater. 19, 3364 (2007).

[51] P. Kumar, S. C. Jain, H. Kumar, S. Chand, V. Kumar, Appl. Phys. Lett. 94, 183505 (2009).

[52] M.S.A. Abdou, F.P. Orfino, Y. Son, S. Holdcroft, J. Am. Chem. Soc. 119 ,4518(1997).

[53] M.G. Matturro, R.P. Reynolds, R.V. Kastrup, C.F. Pictroski, J. Am. Chem. Soc. 108, 2775(1986).

[54] L. Lu¨ er, H.-J. Egelhaaf, D. Oelkrug, G. Cerullo, G. Lanzani, B.-H. Huisman, D. de Leeuw, Org. Electr. 5 ,83(2004).

[55] G. Dennler, C. Lungenschmied, N. S. Sariciftci, R. Schwodiauer, S. Bauer and H. Reiss, Appl. Phys. Lett. 87, 163501 (2005).

[56] J. M. Zhuo, L. H. Zhoa, R. Q. Png, L. Y. Wong, P. J. Chia, J. C. Tang, S. Sivaramkrishna, M. Zhou, E. C. W. Ou, S. J. Chua, W. S. Sim, L. L. Chua and P. K. H. Ho, Adv. Mater. 21, 4747 (2009).

[57] H. H.Liao, C. M. Yang, C. C. Liu, S. F. Horng, H. F. Meng and J. T. Shy, J. Appl. Phys. 103, 104506 (2008)

[58] M. L. Chabinyc, R. A. Stree, J. E. Northrup, Appl. Phys. Lett. 90, 123508 (2007).

[59] Kion Norrman, Morten V. Madsen, Suren A. Gevorgyan, and Frederik C. Krebs, J. AM. CHEM. SOC. 132, 16883–16892(2010)